

DEVELOPMENT AND OPTIMIZATION OF NOVEL TOOLS FOR EXPLORING
RNA-BASED CELL-CELL COMMUNICATION.

by

Cindy T Duong
A Thesis
Submitted to the
Graduate Faculty
of
George Mason University
in Partial Fulfillment of
The Requirements for the Degree
of
Master of Science
Biology

Committee:

_____ Dr. Claudius Mueller, Thesis Director
_____ Dr. Lance Liotta, Committee Member
_____ Dr. Alessandra Luchini, Committee
Member
_____ Dr. Ancha Baranova, Committee Member
_____ Dr. James D. Willett, Director, School of
Systems Biology
_____ Dr. Donna Fox, Associate Dean, Office of
Student Affairs & Special Programs,
College of Science
_____ Dr. Peggy Agouris, Dean, College of
Science

Date: _____ Fall Semester 2015
George Mason University
Fairfax, VA

Development and Optimization of Novel Tools for Exploring RNA-Based Cell-Cell
Communication.

A thesis submitted in partial fulfillment of the requirements for the degree of Master of
Science at George Mason University.

By

Cindy T Duong
Bachelor of Science
George Mason University, 2011

Director: Claudius Mueller, Assistant Professor
Department of Systems Biology

Fall Semester 2015
George Mason University
Fairfax, VA

2015 Cindy T Duong
All Rights Reserved

DEDICATION

I am dedicating this work to my mom and dad. Thank you so much for always supporting me and always being there for me. I would not be where I am today without your love and sacrifice. You are the best parents in the world and I owe my success to you. Therefore, this accomplishment is yours.

ACKNOWLEDGEMENTS

I am very grateful to have an amazing thesis advisor, Dr. Claudius Mueller, for his encouragement, advice, and guidance throughout my research. I would also like to thank Dr. Lance Liotta for the wonderful opportunity to be a part of the Center for Applied Proteomics and Molecular Medicine.

TABLE OF CONTENTS

	Page
LIST OF TABLES	vii
LIST OF FIGURES	viii
ABSTRACT	x
I. INTRODUCTION	10
Chapter 1: Cell-Cell Communication	1
Chapter 2: Ribozymes	3
Chapter 3: Development of RNA Oligonucleotides that Perform Hybridization Chain Reactions in Live Cells	5
Chapter 4: Development of Gene Construct that Causes Cells to Fluorescence upon Receipt of a Trigger RNA	8
II. MATERIALS AND METHODS	11
Gel Electrophoresis	11
Hybridization Chain Reaction	11
Cell Culturing and Reagents	12
Cell Transfection	12
RNA/DNA Extraction	13
Cell Count	14
Restriction Digestion of Plasmid DNA	14
Transcription	14
Plasmid Vectors	15
Cloning	15
Concentration Measurements	16
III RESULTS AND DISCUSSION	17

IV CONCLUSION.....	55
References.....	58
CURRICULUM VITAE.....	61

LIST OF TABLES

Table	Page
Table 1 Hybridization Chain Reaction DNA Candidates	18
Table 2 Hybridization Chain Reaction Sets with Buffer A or B	19
Table 3 Hybridization Chain Reaction RNA Sets with Buffer and Trigger	21
Table 4 Plasmid H1: Expected Size	30
Table 5 Ribozymes PR Size	31
Table 6 HDV Function Test Size	32
Table 7 HHR Function Test Size	32
Table 8 Plasmid H2: Expected Size	35
Table 9 Plasmid HI: Expected Size	35
Table 10 Plasmid H1/H2 PCR Size	39
Table 11 Plasmid C: Expeceted Size	47
Table 12 Amplicon 1 and 2: Expected Size	48
Table 13 Ribozymes Inhibitors	51

LIST OF FIGURES

Figure	Page
Figure 1 Mechanism of Hybridization Chain Reaction	6
Figure 2 Death by Communication	7
Figure 3 Gene Construct	9
Figure 4 Permanent Fluorescent by Communication.....	10
Figure 5 Hybridization Chain Reaction for DNA Candidate Sets	18
Figure 6 Effect of Trigger Concentration and Buffer Type on DNA Oligonucleotide	19
Figure 7 Effect of Trigger Concentration and Buffer Type on DNA Oligonucleotide	21
Figure 8 Transfection of HCR Components in U87MG.....	22
Figure 9 Transfection #2 of HCR Components in U87MG.....	24
Figure 10 Total RNA as HCR Trigger.....	26
Figure 11 Transfection of HCR Components in 4T1 Cells	27
Figure 12 Plasmid H1	28
Figure 13 <i>In vitro</i> Transcription of Plasmid H1.....	30
Figure 14 Amplicon Following PCR	31
Figure 15 <i>In vitro</i> Transcription of Amplicon 1 (HDV).....	32
Figure 16 <i>In vitro</i> Transcription of Amplicon 1 (HHR)	32
Figure 17 Plasmid H2	33
Figure 18 Plasmid I.....	33
Figure 19 <i>In vitro</i> Transcription of Plasmid H1 and Plasmid I.....	35
Figure 20 HCR Combination of H1/H2/I	36
Figure 21 Plasmid H1/H2	37
Figure 22 PCR product of H1/H2	39
Figure 23 PC3 Cells Transfected with Plasmid H1/H2	40
Figure 24 ATG Position in Plasmid A and B	41
Figure 25 Repositioning of ATG using PCR Method	43
Figure 26 Sequencing Analysis of Plasmid B.....	44
Figure 27 Fluorescence Image of Plasmid A	45
Figure 28 Fluorescence Image of Plasmid B	45
Figure 29 Plasmid C.....	46
Figure 30 <i>In vitro</i> Transcription of Plasmid C.....	47
Figure 31 Plasmid C: Amplicon 1 and 2.....	48
Figure 32 <i>In vitro</i> Transcription of Amplicon 1 and 2.....	48
Figure 33 Time Course of Amplicons	49
Figure 34 Structure of Plasmid C Ribozymes.....	50
Figure 35 Inhibitors Complementary to Stemloops of Ribozyme of Plasmid C	51

Figure 36 Ribozyme Cleavage Test of Amplicon 2..... 52
Figure 37 Band Intensity of Ribozyme Cleavage Following Addition of Inhibitors 54

ABSTRACT

DEVELOPMENT AND OPTIMIZATION OF NOVEL TOOLS FOR EXPLORING
RNA-BASED CELL-CELL COMMUNICATION.

Cindy T. Duong, M.S.

George Mason University, 2015

Thesis Director: Dr. Claudius Mueller

Cells communicate by sending and receiving messages that are necessary to carry out essential functions. In cancer, this intricate signaling network of interactions may help tumor cells develop resistance to treatment that could potentially lead to patient death. There are currently no available tools to observe how tumor cells communicate *in vivo*. Here, we developed two tools to visualize RNA-based cell-cell communication, using hybridization chain reactions (HCR) to kill cells that communicate and a Cre-lox gene construct to cause communicating cells to fluoresce.

HCR that exhibited strong polymerization was based on hairpin 1 and 2 (H1/2) loop, stem, toe and overall length, as well as trigger oligonucleotide concentration. However, transfection with HCR components including and excluding a trigger oligonucleotide induced cell death. Plasmids containing targeted HCR component sequences flanked by a 5'-hammerhead ribozyme (HHR) and a 3'-Hepatitis Delta Virus (HDV) ribozyme were created to enable endogenous production of HCR components in

cells. *In vitro* transcription of plasmids indicated ribozyme cleavage and release of target RNA. The H1, H2, and I RNA produced after transcribing the individual plasmids yielded HCR.

Plasmids containing Cre recombinase, ribozyme, LoxP-STOP-LoxP, and green fluorescent protein (GFP) were created to permanently record cell-cell communication. The original gene construct with the start codon (ATG) in front of GFP caused strong false positive fluorescence in cells, while repositioning the ATG in front of LoxP-STOP-LoxP showed a dramatic decrease in fluorescence. To further reduce background fluorescence, a new plasmid was built with HHR at both the 5'- and 3'-end of Cre to ensure Cre gets cleaved and not made into a protein. Inhibitors complementary to the stemloops of each HHR were predicted *in silico* and tested, resulting in one candidate displaying ribozyme cleavage inhibition.

Our studies demonstrate the ability of the HCR mechanism to mediate cell death in cultured human cancer cells. We further developed a Cre recombinase gene construct flanked by two ribozymes that can be specifically inhibited using a short trigger oligonucleotide. Both technologies show promise to become critical tools for visualizing RNA-based cell-cell communication and will be developed further in the future.

I. INTRODUCTION

Chapter 1: Cell-Cell Communication:

A study of cell-cell communication focuses on how cells send and receive messages necessary for them to carry out essential functions. Through communication, cells can establish a tissue, a framework that enables them to work together. In every tissue, cells are engaged in an intricate network of interactions that define biological systems, from plants to animals to bacterial communities. Plant cells cooperate during development¹ and operate as a unit to release hormones that enable the plant to orient itself towards sunlight, while bacterial cells may form biofilms that increase their resistance to antibiotics²⁻⁵. Cancer cells also communicate with one another, and with several kinds of stromal cells, to acquire a specific biological phenotype⁶⁻¹³. However, our knowledge of how this communication network is organized is critically limited because we lack tools to observe and study direct cell-cell communication *in vivo*.

To address this critical need, we have worked on developing two tools that observe and record RNA-based cell-cell communication, using a small non-coding RNA (ncRNA) as signal messenger between cells. Various types of RNA have emerged as a critical and versatile way for cells to communicate and directly influence protein expression in other cells. RNA molecules can pass from cell to cell as cargo of

microvesicles¹⁴, bound to proteins or lipids¹⁵⁻¹⁶, or through gap junctions¹⁷⁻¹⁸. In our first approach, we developed a concept whereby a donor cell expresses and shares a trigger ncRNA (I) with a receiver cell. This initiates a hybridization chain reaction (HCR) in the receiver cell that induces cell death. Our second goal was to develop a reporter that would cause cells to fluoresce permanently following communication, creating a visible snapshot of which cell received communication in the past. A ribozyme within this reporter construct acts as an on/off switch, regulated by the shared trigger RNA. If the trigger RNA inhibits the ribozyme, the ribozyme causes the receiving cell to permanently express green fluorescent protein (GFP), allowing the observation and counting of cells that have received RNA-based communication from specific donor cells in the past.

Chapter 2: Ribozymes

Ribozymes are RNA molecules that have self-processing capacity. Because of their ability to cleave specific sites within a RNA molecule, they may be employed to (a) release specific RNA sequences, and (b) act as an ON/OFF switch for gene expression. Because of sequence requirements and their specific cleavage properties, we chose to use the hammerhead ribozyme (HHR) and hepatitis delta virus (HDV) ribozyme in our constructs.

Hammerhead ribozymes (HHR) were initially discovered in satellite RNAs of small viruses in 1986 for their ability to self-cleave¹⁹. The sequence required for enzymatic activity consists of three stem regions and a central core that is highly conserved²⁰. The hammerhead ribozyme catalyzes and cuts between the guanine and cytosine nucleotides for the 5'HHR and cut between the guanine and uracil for the 3'HHR.

The Hepatitis delta virus (HDV) ribozyme was discovered within the single-stranded RNA of the hepatitis delta virus. This RNA contains self-cleaving activity that is required for replication of the viral RNA²¹. The HDV ribozyme cleaves after any nucleotide other than guanine²². Not having any sequence constraints 5' of the cleavage site makes HDV ribozyme a versatile tool for the creation of synthetic biological constructs.

Incorporating a HHR at the 5'-end of a target transcript and the HDV ribozyme at the 3'-end position²² allowed us to release very specific target RNA molecules from plasmids with nearly no restriction on target RNA sequence. This property of the construct was essential because hybridization chain reactions require specific RNA sequences with no room for variation at either the 5' or 3' end. It should be noted that the ribozymes have been used for similar purposes before²³⁻²⁴. Furthermore, misfolding of ribozymes with the aid of complementary oligonucleotides is known to turn them into efficient ON/OFF switch for downstream protein expression²⁵. In this work, we employed this property of ribozymes for the development of constructs that cause cells to fluoresce when receiving a trigger RNA.

Chapter 3: Development of RNA Oligonucleotides that Perform Hybridization Chain Reactions in Live Cells:

In our first approach to study and visualize RNA-based cell-cell communication, the hybridization chain reactions (HCR) technology was employed. HCR components include two semi-stable, complementary non-coding RNA molecules, Hairpin 1 (H1) and Hairpin 2 (H2), and a small trigger RNA (I). Each HCR hairpin contains a long stem and a short loop and toe²⁶. Without the trigger RNA present, H1 and H2 are stable and do not hybridize with one another (Figure 1A). Hybridization of the trigger RNA to the toe and part of the stem of H1 opens and exposes the rest of H1 for further hybridization. Newly exposed part of H1 hybridizes to the toe and stem of H2, which leads to exposition of the end of H2 that binds and opens another H1 molecule, thus, propagating a chain reaction of hybridization events between the two hairpins to form a long, double-stranded RNA (dsRNA)²⁶ (Figure 1 B).

Within the cell, the formation of dsRNA stimulates the innate immune system, leading to the activation of protein kinase R (PKR). PKR contains two domains: an N-terminal dsRNA binding domain and a C-terminal kinase domain. PKR plays an important part in protecting mammalian cells against viral infection²⁷⁻²⁹. When activated by double-stranded RNA, PKR inhibits protein synthesis and induces apoptosis. In our system, receiver cells that express double stranded complexes of H1 and H2 would, therefore, die following communication with donor cells expressing the trigger RNA (Figure 2).

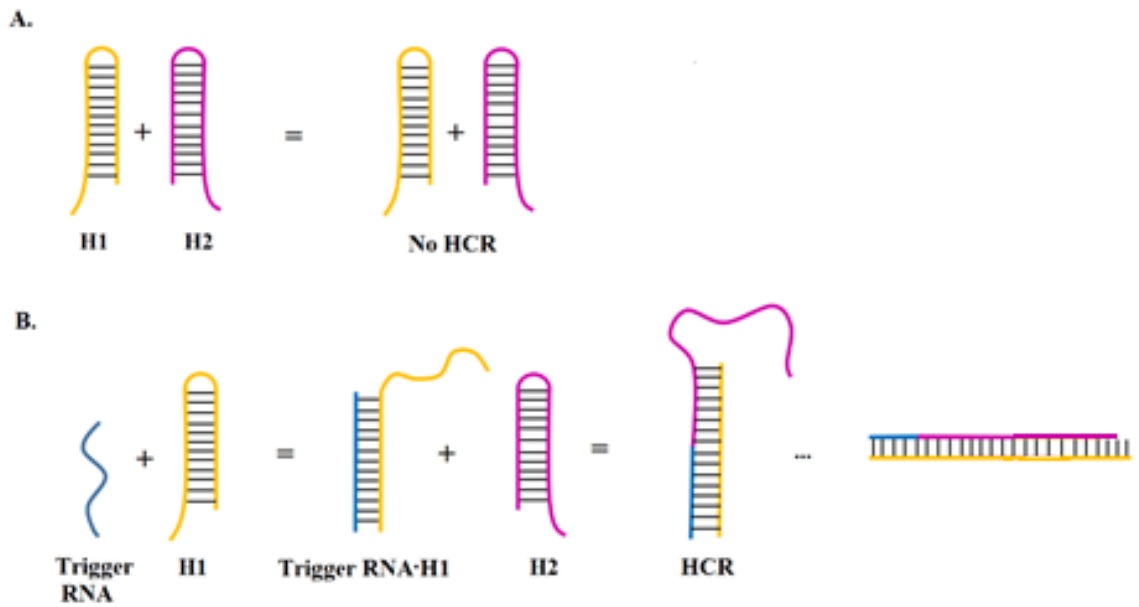


Figure 1: Mechanism of hybridization chain reactions. (A) Hairpin 1 (H1) and hairpin 2 (H2) are stable in the absence of trigger RNA (no HCR). (B) In the presence of a trigger RNA, H1 will bind the trigger and unfold. This permits the subsequent unfolding and hybridization of H1 and H2 hairpins to each other, resulting in long strands of double-stranded RNA.

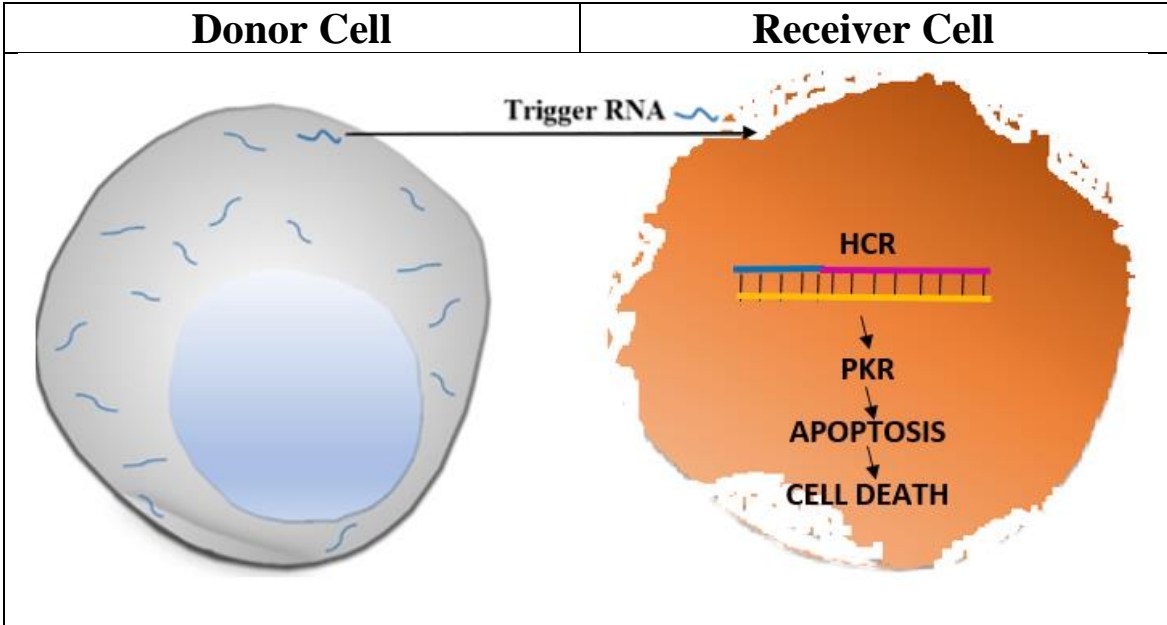


Figure 2: A donor cell shares a trigger RNA with a receiver cell, initiating HCR. The resulting double-stranded RNA within the receiver cell activates protein kinas R (PKR), that, in turn, induces apoptosis in the receiver cell.

Chapter 4: Development of Gene Construct That Causes Cells to Fluorescence upon Receipt of a Trigger RNA:

In our second approach to visualize RNA-based cell-cell communication, we developed a reporter that induces permanent fluorescence following the receipt of a specific trigger RNA. This RNA-based cell-cell communication technology causes cells to fluoresce permanently following the receipt of a specific trigger RNA. The receiving cell contains a Cre-recombinase-ribozyme-LoxP-STOP-LoxP-green fluorescent protein construct (Figure 3). Within this construct, there is a ribozyme capable of cleaving specific locations within the RNA sequence, therefore destabilizing Cre recombinase mRNA and inhibiting Cre expression. Cre catalyzes the recombination of DNA between specific sites called loxP sequences, which contain binding locations for Cre. In our gene construct, a stop codon is inserted between two loxP sites in front of green fluorescent protein (GFP)³⁰. GFP is a protein that exhibits bright green fluorescence when exposed to light in the blue to ultraviolet range.

Communication is established between donor cells and receiver cells upon receipt of the donor trigger ncRNA. Once accepted by the receiver cells, the trigger RNA binds to the ribozyme stemloop and causes the ribozyme to misfold, suppressing ribozyme activity. As a result, the ribozyme in the gene construct is unable to cleave Cre messenger RNA. Once the ribozyme is inactivated and no longer cleaving, Cre protein is expressed. This leads to the permanent removal of the stop codon located in front of the green fluorescent protein. Therefore, GFP will be expressed, enabling us to visualize and count

the cells that have received RNA-based communication from donor cells in the past (Figure 4).



Figure 3: Gene construct containing Cre recombinase, ribozyme, loxP/STOP sites and green fluorescent protein for permanently marking cells receiving RNA-based communication.

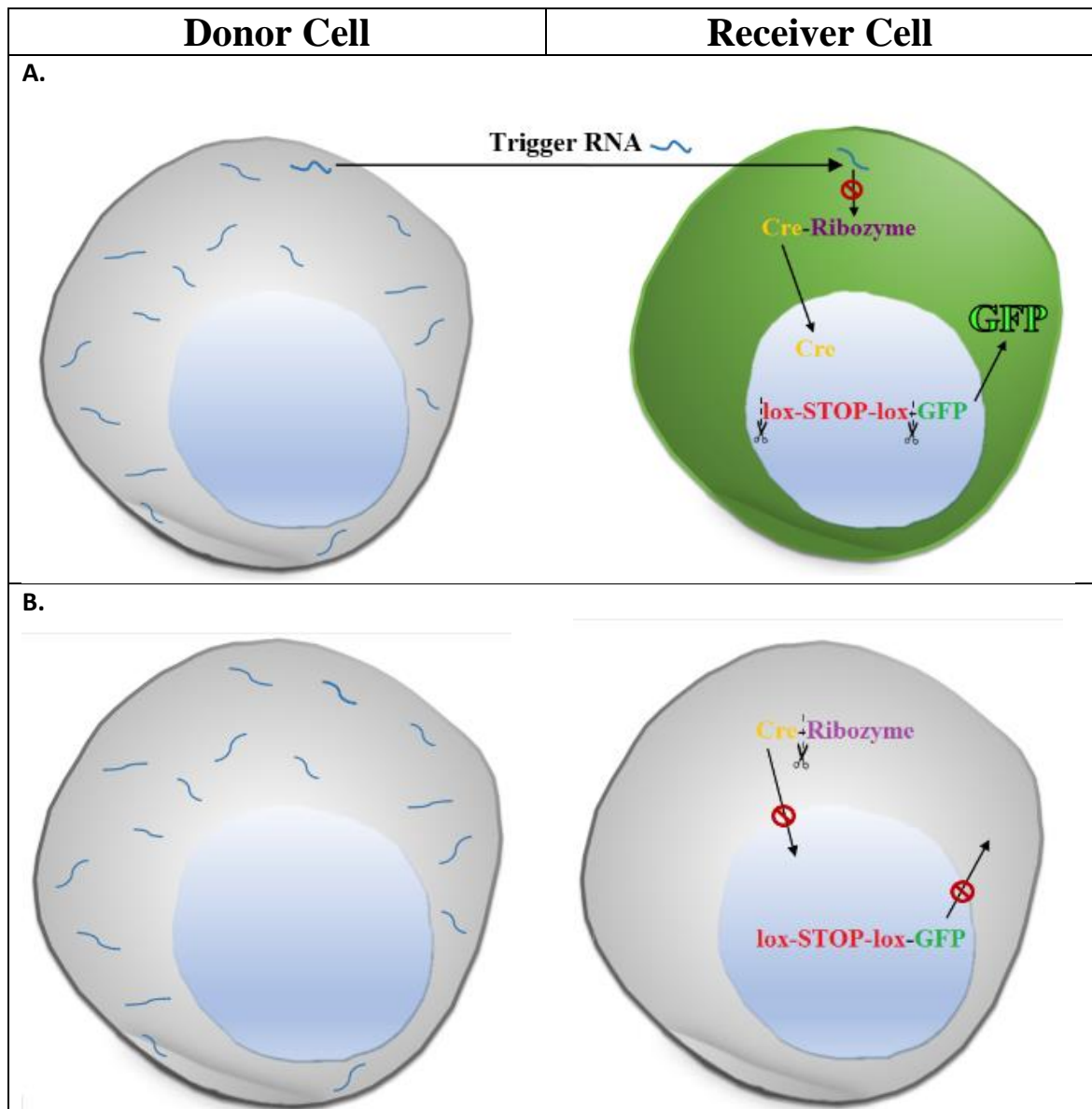


Figure 4: Mechanism of permanently recording RNA-based cell-cell communication. (A) Receiving a trigger RNA will aid in misfolding the ribozyme, precluding the ribozyme-guided cleaving of Cre. Hence, Cre recombinase will be active, resulting in the removal of lox-STOP-lox and leading to green fluorescent protein expression. (B) When communication is nonexistent between the donor and receiver cell, no trigger RNA is shared and the ribozyme will continue to destabilize Cre mRNA.

II. MATERIALS AND METHODS

Gel Electrophoresis:

Either 0.7%, 1.5%, or 2% agarose gels (depending on the size of desired sample) containing 0.1 μ l of ethidium bromide per ml of gel volume were prepared using TBE buffer (Thermo Fisher Scientific, Inc., Waltham, MA), low-melting agarose and diethylpyrocarbonate treated water. Agarose gels were ran at 100 V for 45 minutes and visualized under ultraviolet light. Native and denaturing polyacrylamide gels that were purchased precast (Thermo Fisher Scientific, Inc., Waltham, MA) and run at 150 V for 45 minutes in 1xTBE, stained for 30 minutes in a solution containing 0.1 μ l of SYBR Gold per ml of TBE buffer, and viewed under ultraviolet light.

Hybridization Chain Reaction:

Oligonucleotide sets that were developed to perform hybridization chain reaction were generated using an in-house developed bioinformatics software. Oligos were custom made by Thermo Fisher Scientific (Waltham, MA) or Integrated DNA Technologies (Coralville, IA). Selected sets of hairpin 1, hairpin 2, and trigger DNA were combined in a 2:2:1 ratio in a test tube. The reaction mixes were incubated for one hour at 37°C in reaction buffer made with 50 mM Na₂HPO₄ and 0.5 M NaCl²⁶. Optimally

reacting H1, H2, and I oligonucleotides were transcribed to RNA and transfected into cancer cell lines to observe induction of cell death.

Cell Culturing and Reagents:

Human prostate cancer PC-3 (ATCC® CRL-1435™) were maintained in F-12K culture medium, mouse breast cancer 4T1 (ATCC® CRL2539™) were kept in RPMI-1640 medium, and human glioblastoma cells U-87 MG (ATCC® HTB14™) were grown in MEM medium (Gibco/Invitrogen). The complete growth medium were supplemented in each case with fetal bovine serum (FBS) to a final concentration of 10%. Cells were kept at 37°C and 5% CO₂. After cultivation, cells were detached with 0.05% trypsin/0.02% EDTA (ATCC) and washed with PBS.

Cell Transfection:

Cells were transfected using either Lipofectamine 3000, Oligofectamine (Thermo Fisher Scientific, Inc., Waltham, MA), or Xfect Transfection Reagent (Clontech Laboratories, Mountain View, CA) according to manufacturer recommendations. The respective transfection complexes were added to cells at about 50% confluency.

RNA/DNA Extraction:

Total RNA was extracted using the Quick-RNA™ MicroPrep Kit (Zymo Research, Irvine, CA) following the manufacturer's recommendations. In short, RNA was extracted by adding 2 volumes of buffer/ethanol to the sample. The mixture was transferred to a Zymo-Spin™ Column and centrifuged for 30 seconds. 400 µl of RNA Prep Buffer was added to the column and centrifuged for 30 seconds. Next, 700 µl RNA Wash Buffer was added to the column and centrifuged for 30 seconds. The columns were placed in an RNase-free tube and 15 µl of DNase/RNase-Free Water was used to elute the RNA.

The DNA Clean & Concentrator™ kit (Zymo Research, Irvine, CA) was used to extract DNA. The DNA sample was mixed with 3 volumes of DNA Binding Buffer and transferred into a Zymo-Spin™ Column and centrifuged for 30 seconds. 200 µl of DNA Wash Buffer were then added to the column and centrifuged for 30 seconds. The wash step was repeated to ensure complete removal of the wash buffer. A total of 6 µl of DNA Elution Buffer were added to the column matrix and incubated at room temperature for one minute. The columns were then transferred to a 1.5 ml microcentrifuge tube and centrifuged for 30 seconds to elute the DNA.

Cell Counts:

The alamarBlue® Assay from Thermo Fisher Scientific Inc. (Waltham, MA) was used to estimate cell viability. In short, 10 µl of alamarBlue were added per 100 µl of media to each well of a clear, flat bottom microplate. Following incubation for three hours fluorescence was analyzed at 570/585 nm excitation/emission wavelengths.

Restriction Digestion of Plasmid DNA:

Restriction enzymes and buffer were purchased from New England Biolabs (Ipswich, MA) and mixed gently according to manufacturer recommendations with template DNA before incubation at 37°C for 1 hour.

Transcription:

Transcription was carried out using the MAXIscript® SP6 Transcription Kit and MAXIscript® T7 Kit from Applied Biosciences (Foster City, CA), according to the manufacturer's protocol. The components of the reaction included nuclease-free water, DNA template, 10x Transcription Buffer, ATP, CTP, GTP, UTP, and enzyme mix (T7 or SP6). The solutions were mixed thoroughly and incubated for 5 minutes to 4 hours, depending on the respective experiment, at 37°C. Next, 1 µl TURBO DNase was added to the solution incubation extended at 37°C for 15 minutes. To stop the reaction, 1 µl of 0.5 M EDTA were added to each sample.

Plasmid Vectors:

The plasmid vectors used for all experiments were either pcDNA3.1(-) (Thermo Fisher Scientific, Inc., Waltham, MA) or the Tet-One™ Inducible Expression System (Clontech Laboratories, Mountain View, CA).

Cloning:

Cloning was performed using the In-Fusion® HD Cloning Kit (Clontech Laboratories, Mountain View, CA). Unpurified PCR products were treated with Cloning Enhancer and incubated at 37°C for 15 minutes, followed by 80°C for 15 minutes in a PCR thermal cycler. The In-Fusion cloning reaction mixture was incubated for 15 minutes at 50°C, then placed on ice. Transformation was accomplished using Stellar Competent cells. 50 µl of cells were placed into a 14 ml round-bottom tube. No more than 5 µl of In-Fusion-cloning reaction were added to 14 ml tube containing the cells. This mixture was placed on ice for 30 minutes, heat shocked at 42°C for 45 seconds and placed on ice again for 2 minutes. SOC medium was added to bring the final volume of the mixture to 500 µl. The mixture was incubated by shaking (225 rpm) for 1 hour at 37°C. The transformation reaction was diluted according to the desired concentration with LB broth (1:100, 1:20, 1:5, concentrated plate) and the mixture spread on plates containing 50 µg/ml ampicillin in agar. The plates were incubated overnight at 37°C. The following day, isolated colonies were picked and swirled in 100 ml LB broth containing 25 µg/ml ampicillin and incubate 37°C overnight.

Concentration measurements:

The concentrations of RNA and DNA samples were measured using the Qubit™ fluorometric quantitation from Thermo Fisher Scientific (Waltham, MA), with the instrument at room temperature (22-28°C). The mixture was incubated in clear PCR tubes for 2 minutes. For each measurement, the Qubit was first calibrated using the appropriate standards before measuring sample concentrations.

Gel images were taken using a FluorChem™ R system imager from Protein Simple (San Jose, CA) at a wavelength of 593 nm. The detected bands were quantified using Fiji³¹. Fluorescence microscopy was performed using an Olympus microscope with a FITC filter option (Olympus America Inc., Center Valley, PA).

III RESULTS AND DISCUSSION

Development of RNA Oligonucleotides that Perform Hybridization Chain Reactions in Live Cells:

Ten candidate sets of oligonucleotides with different combinations of trigger and hairpin lengths (Table 1) were tested in hybridization chain reaction (HCR). During the selection process, DNA oligonucleotides were utilized, as DNA is less expensive compared to RNA, while having similar hybridization characteristics. Reactions were performed with a 2:2:1 ratio of hairpin 1, hairpin 2, and trigger DNA. The candidates were combined in a test tube and incubated at 37°C for 1 hour in reaction (50 mM Na₂HPO₄ and 0.5 M NaCl¹⁰). Strongest polymerization (indicating a successful HCR) was observed in sets 6, 9, and 10 with hairpin sites of trigger, stem, loop, and toe that are typically larger in length (Table 1, Figure 5). HCR production was reduced with trigger oligonucleotide lengths less than 20 base pairs (bp) and stems with lengths less than 14 bp. Oligonucleotide sets 1, 2, and 3, with very short trigger, stem, and loop lengths showed no polymerization (Figure 5, Table 1).

Table 1: Size parameters (stem, loop, toe) of ten trigger, hairpin 1 and hairpin 2 DNA oligonucleotides sets.

Hybridization Chain Reaction DNA Candidates				
Set	Trigger [bp]	Hairpin 1 and 2		
		Stem [bp]	Loop [bp]	Toe [bp]
1	10	6	4	4
2	10	6	4	4
3	10	6	4	4
4	20	16	4	4
5	20	16	4	4
6	20	14	6	6
7	18	14	4	4
8	18	14	4	4
9	24	18	6	6
10	24	18	6	6

Hybridization Chain Reaction Products for DNA Candidate Sets

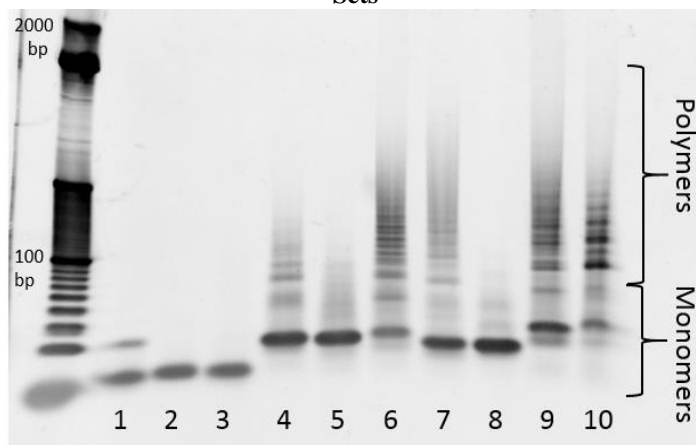


Figure 5: Hybridization chain reaction products for hairpin 1, hairpin 2, and trigger DNA candidate sets (see Table 1).

Once candidates that yielded efficient hybridization chain reaction were identified, the effect of different reaction buffers and trigger concentrations were tested on the selected sets (4, 5, 6, 7, and 8). Buffer A contained 50 mM Na_2HPO_4 and 0.5 M NaCl^{26} . Buffer B consisted of 20 mM Heps pH 7.5, 4 mM MgCl_2 and 100 mM KCl^{32} . A total of 20 combinations of different sets, reaction buffers, and trigger concentrations were tested (Table 2). The two native polyacrylamide gels in Figure 6 demonstrate strong HCR in sets that contained buffer A. Equally important, higher trigger concentration (0.4 μM) resulted in greater polymerization while lower trigger concentration (0.04 μM) lead to reduced HCR. Finally, we showed that hairpin 1 and 2 when combined together do not

hybridize in the presence of limited trigger concentration. We conclude that the presence of a high trigger concentration is necessary for successful HCR.

Table 2: Sample of twenty HCR reactions with different trigger concentrations (low = 0.04 μ M, high = 0.4 μ M) and buffers (for set parameters see Table 1).

Hybridization Chain Reaction DNA Sets with Buffer A or B			
Reaction Number	Set	Buffer Type	Trigger Concentration [μ M]
1	4	A	0.4
2	4	A	0.04
3	4	B	0.4
4	4	B	0.04
5	5	A	0.4
6	5	A	0.04
7	5	B	0.4
8	5	B	0.04
9	6	A	0.4
10	6	A	0.04
11	6	B	0.4
12	6	B	0.04
13	7	A	0.4
14	7	A	0.04
15	7	B	0.4
16	7	B	0.04
17	8	A	0.4
18	8	A	0.04
19	8	B	0.4
20	8	B	0.04

Effect of Trigger Concentration and Buffer Type on DNA Oligonucleotide Sets

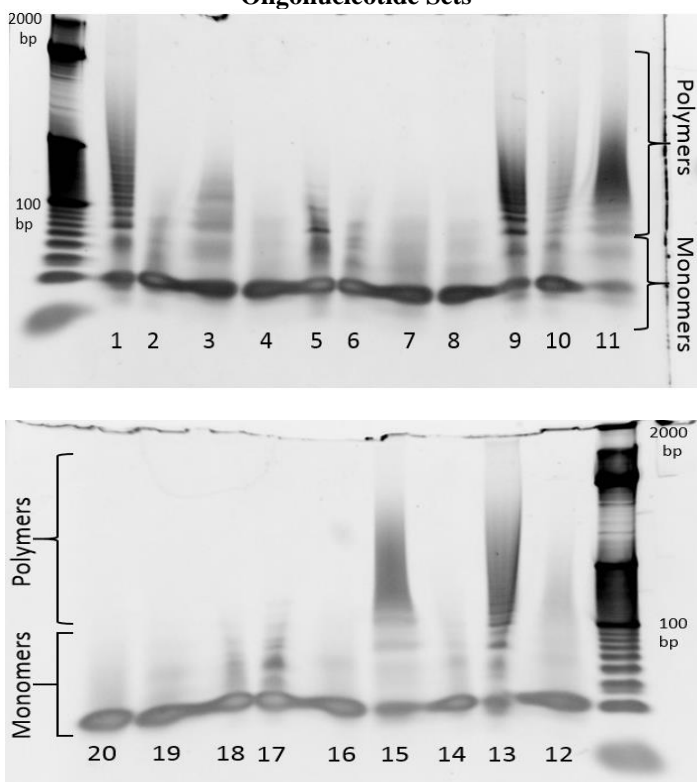


Figure 6: Hybridization chain reaction products of twenty reactions differing in oligonucleotide set, trigger concentration and buffer (see Table 2). Sets with buffer A and high trigger concentration showed the highest amount of DNA polymerization.

A working model showing polymerization was observed using DNA oligonucleotides (Figure 5, 6). The next objective was to emulate the same HCR effect in RNA oligonucleotide sets as well as test the effect of different concentrations of buffer A and trigger RNA. Strongest HCR was shown in reaction 2, containing buffer A at a high

concentration and 0.4 μM of trigger RNA (Table 3 and Figure 7: lane 2). The experiment indicated that HCR can be accomplished by using RNA oligonucleotides. It is clear that higher buffer concentration and trigger concentration led to stronger polymerization.

Table 3: Combinations of buffer and trigger concentrations used.

Hybridization Chain Reaction RNA Sets with Buffer and trigger concentrations		
Reaction Number	Reaction Buffer A Concentration	Trigger Concentration [μM]
1	Low	0.4
2	High	0.4
3	Low	0.1
4	High	0.1

Effect of Trigger Concentration and Buffer Type on RNA Oligonucleotide Sets

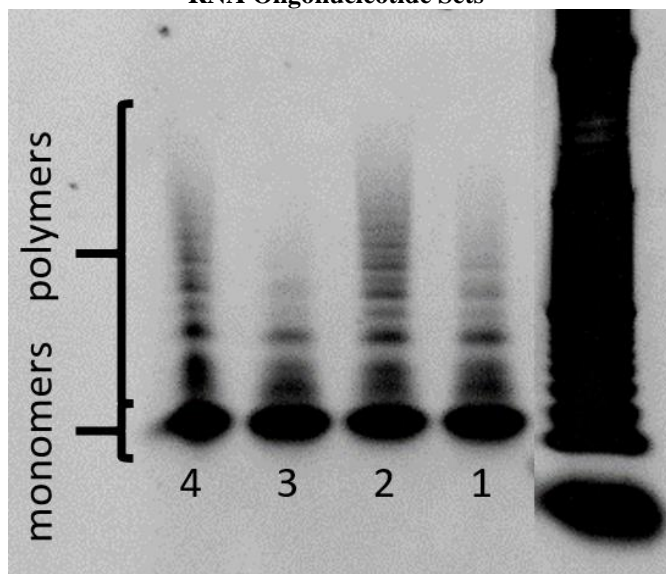


Figure 7: Hybridization chain reaction products for RNA oligonucleotide sets (see Table 3).

In prior experiments, we were able to demonstrate that HCR amplification proceeds in test tubes. To test whether HCR would proceed *in vivo*, the same HCR mechanism was evaluated in live cells through induced cell death. U87MG cells were transfected with HCR components using Lipofectamine® 3000 Reagent. Cells either received no treatment, transfection reagent only, H1/H2, or H1/H2/I components. Cell death was determined by fluorescence level where the samples were replicated 6 times in a 96-well plate. The average fluorescence values of transfected U87MG cells were: no treatment: 12,845.55, treatment with transfection reagent only: 13,517.71, H1/H2: 5,154.88, H1/H2/I: 3,092.25 (Figure 8). Cells that received no treatment and cells treated with transfection reagent only had higher fluorescence as compared to H1/H2 and

H1/H2/I treated cells. Cells that underwent H1/H2/I transfection showed low fluorescence, indicating cell death. However, transfecting cells with H1 and H2 together should not have resulted in low fluorescence value, indicating that HCR may occur in absence of trigger RNA.

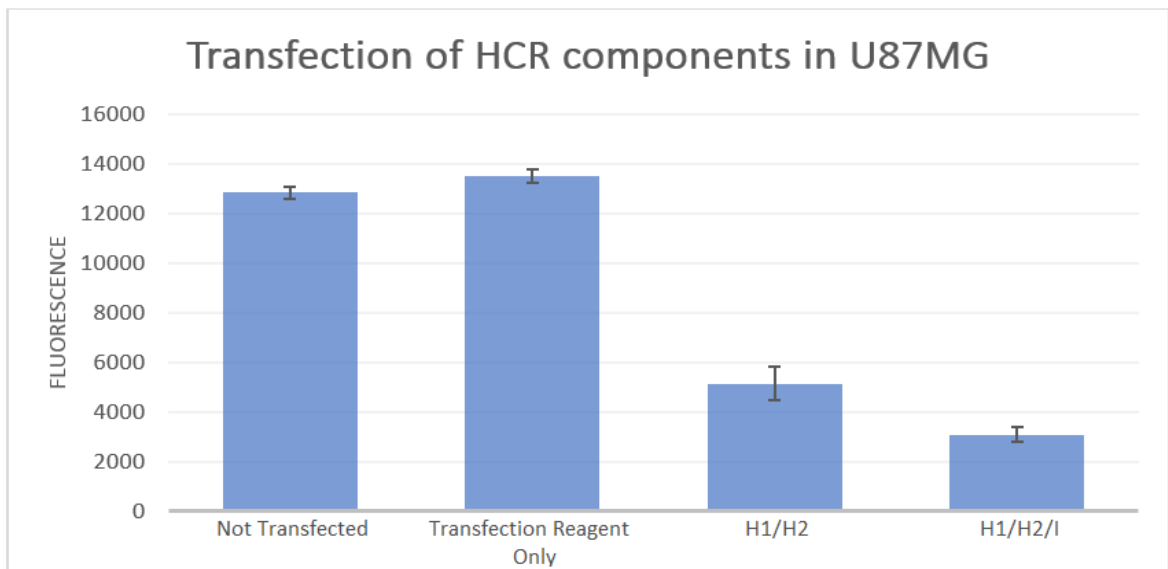


Figure 8: Cell viability of U87MG cells transfected with a complete set of HCR components (H1/H2/I), only hairpins 1 and 2 without trigger (H1/H2), transfection reagent only or not transfected.

A second transfection test was conducted to determine whether cell death was the consequence of HCR in the absence of trigger RNA, or rather due to general toxicity of H1 or H2 (Figure 8). Figure 9 shows the relative viability of U87MG cells that received either transfection reagent only, H1, H2, H1/H2, or H1/H2/I. Fluorescence values were calculated based on the average of samples replicated 6 times in a 96 well plate. Cells

that received transfection reagent only, H1, and H2 had fluorescence values of 24947.44, 23087.94, 24006.55, respectively, which were much higher as compared to that of cells that received H1/H2 and H1/H2/I transfections, with respective fluorescence values of 3057.87, 2207.32. Based on the results described above, the transfection reagent, and the addition of individual HCR components did not induce U87MG cell death. Individual transfection of H1 and H2 components caused no substantial reduction in population of cells, while cells transfected with H1/H2 and H1/H2/I combinations of oligonucleotides showed a decrease in their viability. These results suggest that interactions between H1 and H2 may play a role in mediating cell death, and that HCR is actually occurring in cells containing H1/H2.

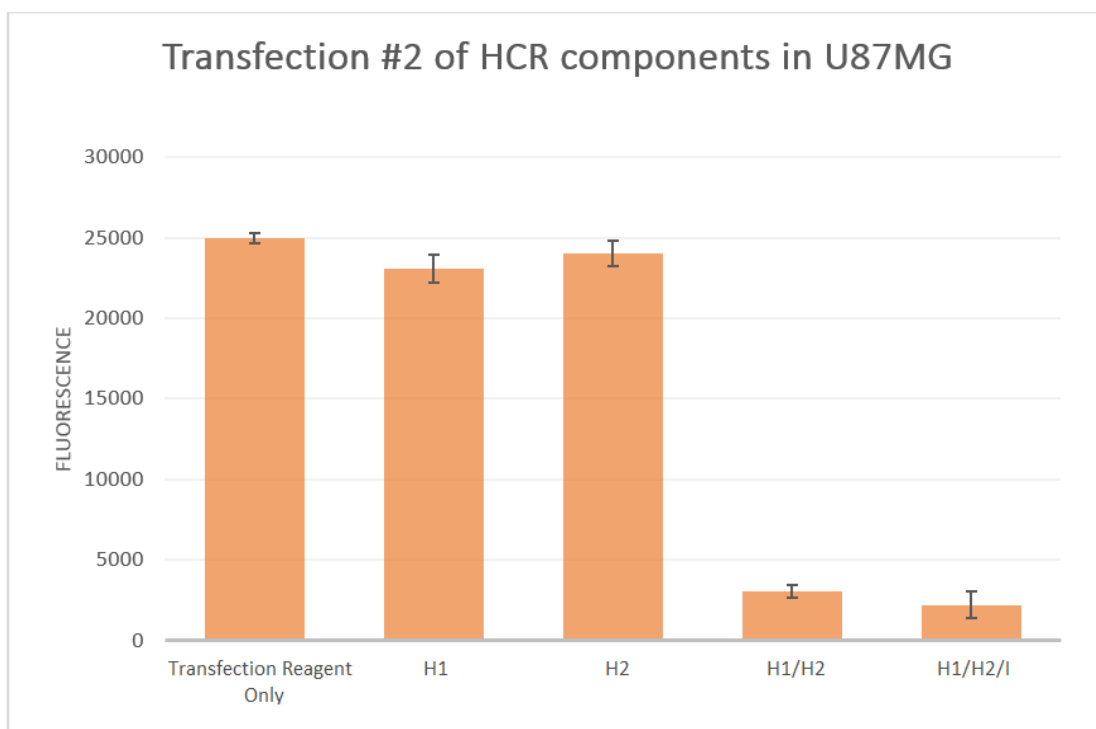


Figure 9: Cell viability of U87MG cells transfected with a complete set of HCR components (H1/H2/I), only hairpins 1 and 2 without trigger (H1/H2), only a single hairpin (H1 or H2), or only transfection reagent.

In previously described HCR test tube experiments, H1 and H2 alone failed to polymerize. However, as soon as H1 and H2 were placed into cells, the hairpins interacted and formed HCR. Therefore, we hypothesized that the cell's total RNA may act as a trigger for HCR formation. In order to test this hypothesis, we extracted total RNA from cells and combined it with chain reaction components. Testing HCR efficiency in presence of total cellular RNA was performed using oligonucleotide set 6, because this set yielded the most efficient HCR in our previous experiments (Table 1 and Figure 5). As demonstrated in Figure 10, strong polymerization was seen when

combining H1/H2 and I DNA (lane 1). Replacing trigger DNA with total RNA from 4T1 (lane 2) or U87MG (lane 3) cells shorter oligonucleotide polymers, as compared to total RNA alone (lanes 4 and 5). This indicates that HCR formation is more efficient in the presence of a specific trigger oligonucleotide than in presence of total RNA, but HCR can also proceed when H1 and H2 components are mixed with total cellular RNA.

Total RNA as HCR Trigger

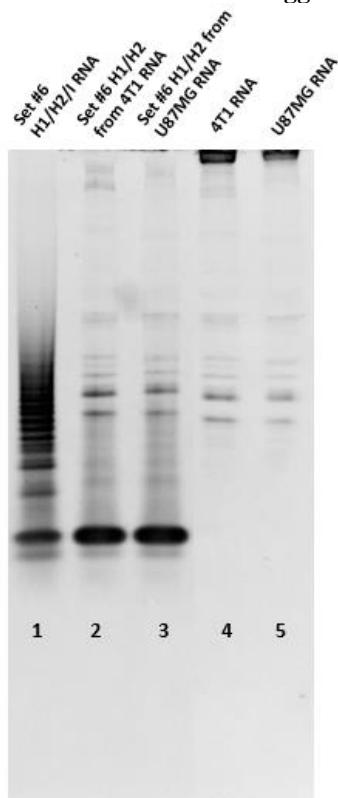


Figure 10: Hybridization chain reaction products is presence of total cellular RNA as trigger (lane 1: HCR set 6 H1/H2/I; lane 2: H1/H2 RNA of HCR set 6 plus total RNA from 4T1 cells; lane 3: H1/H2 RNA of HCR set 6 plus total RNA from U87MG cells; lanes 4 and 5: total RNA from 4T1 and U87MG cells, respectively).

Prior transfection tests were carried out in U87MG cells. We wanted to see if HCR components would perform in a similar way, when transfected into 4T1 cells. Thus, three arms of experiment were run using 4T1 cells: not transfected, treated with transfection reagent only, or transfected with H1/H2/I. The average fluorescence values (n=6) were 25193.16, 27824.12, and 19885.24 for no treatment, transfection reagent only, and transfection with H1/H2/I, respectively (Figure 11). The reduced impact of HCR on 4T1 cell viability indicates that efficiency of HCR depends on the characteristics of the cell line.

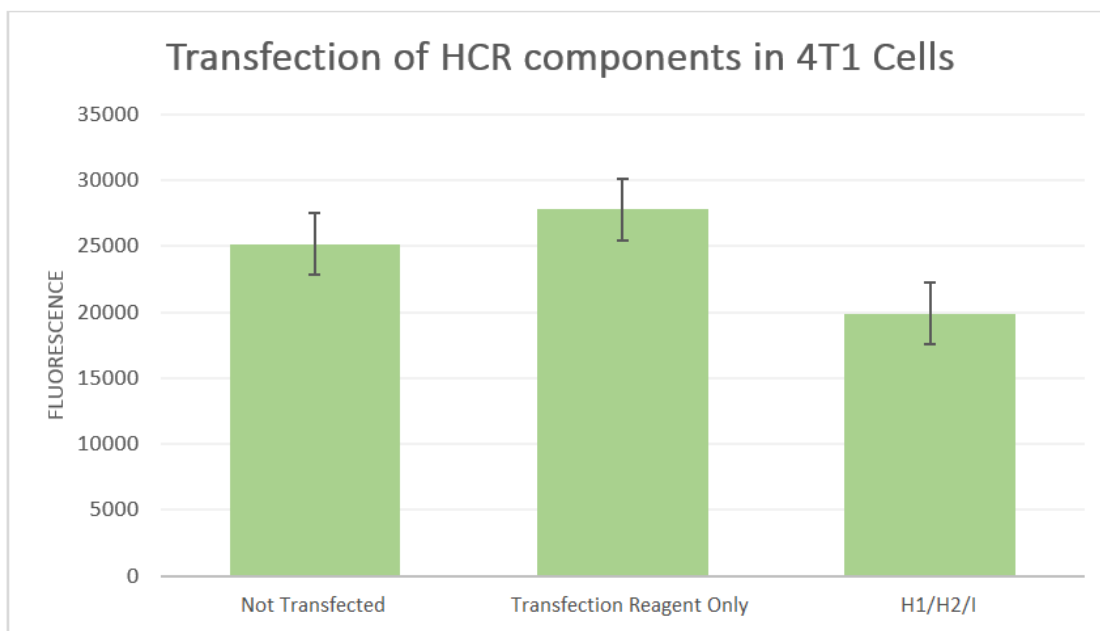


Figure 11: Cell viability of 4T1 cells transfected with a complete set of HCR components (H1/H2/I), transfection reagent only or not transfected.

Up to this point, our studies were carried out either in test tubes or by transfecting synthetic HCR components into cells. Our next goal was to make living cells produce their own HCR components. In order to accomplish this, we designed the recombinant plasmids to produce the sequences of interest. The first of the plasmids we designed (Plasmid H1) contained a T7 promoter for *in vitro* transcription, a HHR 5' of our sequence of interest (H1), and a HDV ribozyme at the 3'-end position (Figure 12). In addition, an in-fusion overlap was placed in front of an XhoI restriction enzyme site, which was necessary for successful In-Fusion Cloning. Restriction enzyme sites for XhoI

and HindIII were used to linearize the vector. In addition, to ensure proper folding of the ribozyme, a spacer was inserted in front of the HHR. Lastly, Plasmid H1 contained an antibiotic resistance marker for recombinant cell selection.

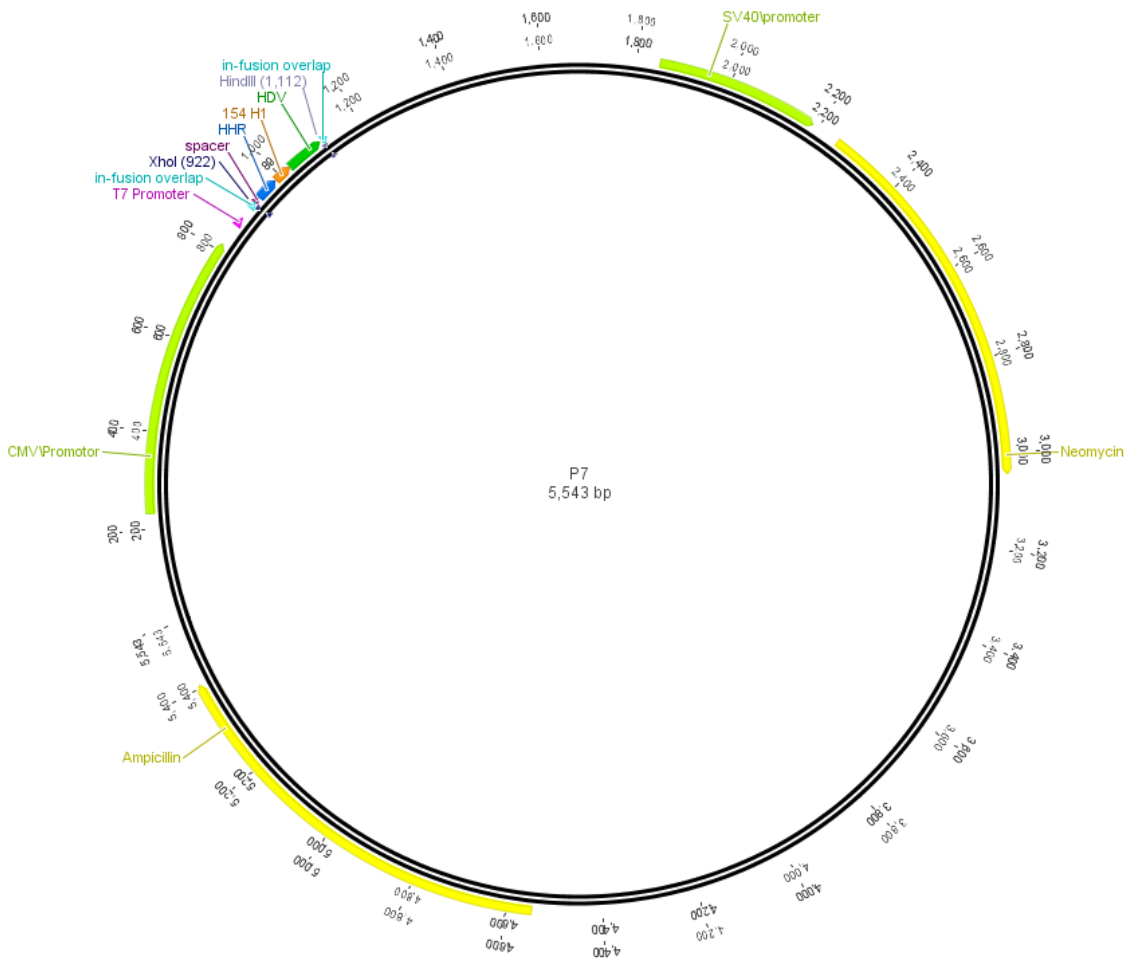


Figure 12A: Plasmid H1 with a CMV promoter, T7 promoter, hammerhead ribozyme (HHR), hairpin 1 (H1), and hepatitis delta virus ribozyme (HDV). The construct used a pcDNA3.1(-) vector as a backbone.

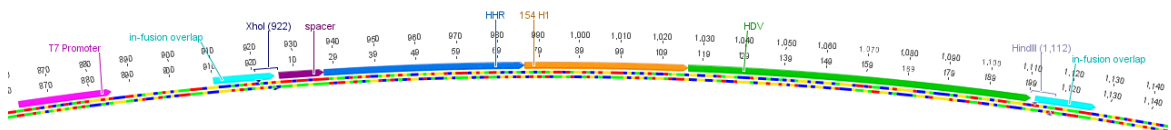


Figure 12B. Plasmid H1 insert, including hammerhead ribozyme (HHR, blue), hairpin 1 (H1, orange), and hepatitis delta virus ribozyme (HDV, green).

Once Plasmid H1 was created, three clones were selected and sent for Sanger DNA sequencing. To evaluate the cleavage with ribozyme, the DNA of the plasmid H1 (clone 1, 2, and 3) was transcribed (Table 4 and Figure 13). As shown in Figure 13, a product of cleavage was observed, 40 bp in size, indicating that the target sequence (H1) was cleaved out, and that both ribozymes cleave in proper site. However, the efficiencies of the cleavage for individual ribozymes were difficult to evaluate due to similarity in product sizes for HHR and HDV cleavage. Correct HHR cleavage would result in a 107 bp fragment (T7 promoter to the end of HHR), while HDV cleavage would result in an 85 bp fragment (HDV cleaved to HindIII cut site).

Table 4: Expected size of all possible cleavage fragments of *in vitro* transcribed Plasmid H1.

Plasmid H1: Expected Size	
Size [bp]	Explanation
235	T7 to HindIII cut site
40	H1 (HHR/HDV cleaved)
107	T7 to HHR cleaved
85	HDV cleaved to HindIII cut
125	H1 + HDV to HindIII cut (no HDV cleavage)

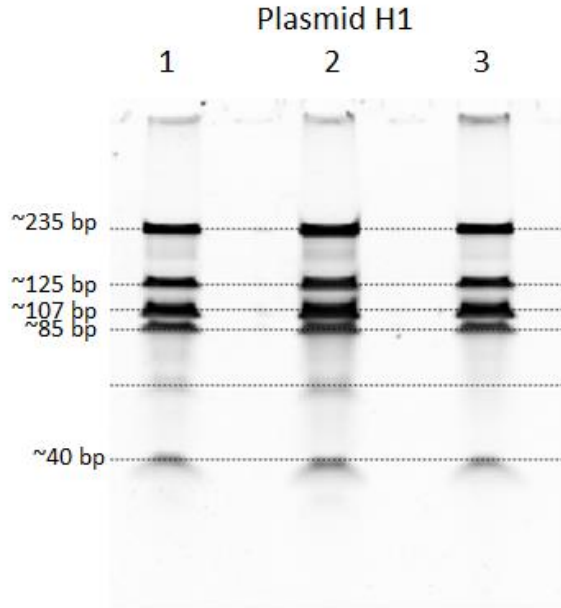


Figure 13: Ribozyme cleavage fragments following *in vitro* transcription of clones 1, 2 and 3 of plasmid H1.

In order to separately evaluate the efficiency of each ribozyme, we compared native ribozyme function to mutated ribozymes. First, HDV was mutated by eliminating 6 bp from its 3' section, causing the ribozyme to fold differently and interrupting its ability to cleave. To mutate the HHR, 7 bp were removed from the catalytic core, causing the ribozyme to become inactive. Table 5 and Figure 14 show the expected PCR product size of the ribozymes and their respective mutated sequence. PCR products of H1+HDV were observed at 147 bp, with the mutated H1+HDV sequence at a slightly lower size (136 bp). The H1+HHR amplicon and its mutated sequence were observed at 119 bp and 112 bp, respectively. However, the band that corresponds to HHR was not as strong and specific compared to the HDV PCR products.

Table 5: Expected amplicon size following PCR of H1 plasmid. Amplicons include hairpin 1 (H1) and either wildtype or mutated hammerhead ribozyme (HHR) or hepatitis delta virus ribozyme (HDV).

Ribozymes PCR Size	
Size [bp]	Explanation
147	H1 + HDV
136	H1 + HDV mutated
119	H1 + HHR
112	H1 + HHR mutated

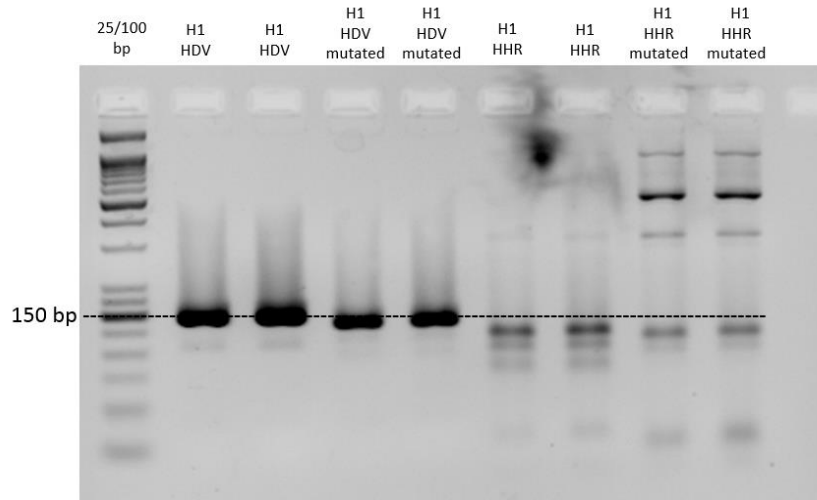


Figure 14: Amplicons following PCR of H1 plasmid. Amplicons include hairpin 1 (H1) and either wildtype or mutated hammerhead ribozyme (HHR) or hepatitis delta virus ribozyme (HDV).

The PCR bands were then cut from the agarose gel, cleaned, and transcribed to test the function of the ribozymes. As seen by the 125 bp fragment in Figure 15 and Table 6, the efficiency of HDV cleavage and subsequent H1 release is somewhat limited. Nevertheless, the evidences of cleavage were clearly observed (see HDV fragment at 85 bp and H1 fragment at 40 bp). No cleavage was detected in mutated HDV.

Similarly, mutated HHR did not cleave, as indicated by a single 95 bp band (Figure 16). However, non-mutated HHR demonstrated complete cleavage with products at 62 bp (HHR) and 40 bp (H1) and no band at 102 bp (Table 7). Therefore, HHR was more efficient at cleaving and releasing our desired product compared to HDV.

Table 6: Expected cleavage fragments following in vitro transcription of H1 amplicons. Amplicons include hairpin 1 (H1) and either wildtype or mutated hepatitis delta virus ribozyme (HDV).

HDV Function Test	
Size [bp]	Explanation
125	H1 + HDV
119	H1 + HDV mutated
85	HDV
40	H1

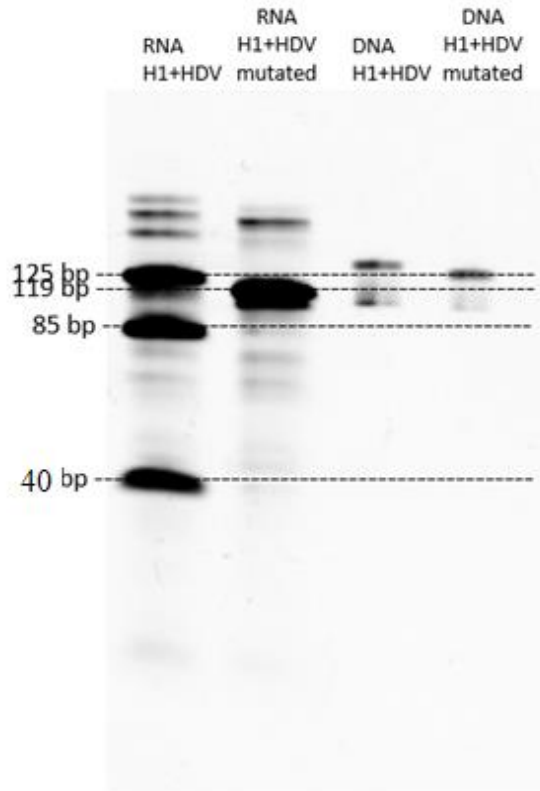


Figure 15: Cleavage fragments following in vitro transcription of H1 amplicons. Amplicons include hairpin 1 (H1) and either wildtype or mutated hepatitis delta virus ribozyme (HDV).

HHR Function Test	
Size [bp]	Explanation
102	H1 + HHR
95	H1 + HHR mutated
62	HHR
40	H1

Table 7: Expected cleavage fragments following in vitro transcription of H1 amplicons. Amplicons include hairpin 1 (H1) and either wildtype or mutated hammerhead ribozyme (HHR).

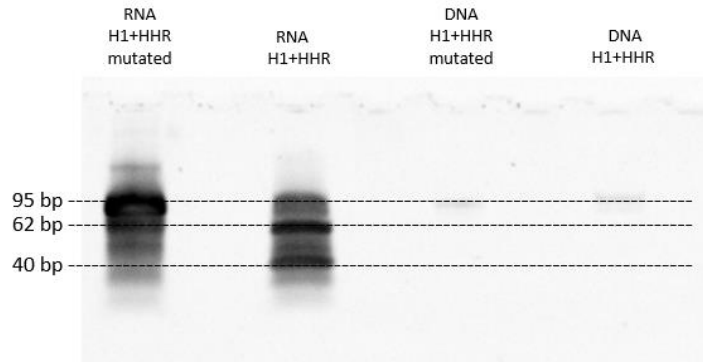


Figure 16: Cleavage fragments following in vitro transcription of H1 amplicons. Amplicons include hairpin 1 (H1) and either wildtype or mutated hammerhead ribozyme (HHR).

As described above, we were able to successfully build Plasmid H1 with flanking ribozymes that were able to cleave and release our H1 target sequence. Therefore, we used a similar plasmid structure for the remaining HCR components. Figure 17 and Figure 18 show the schematic of the newly created plasmids, Plasmid H2 and Plasmid I. As in Plasmid H1, the insert in Plasmid H2 and Plasmid I included the target sequence flanked by a 5' hammerhead ribozyme and a 3' HDV ribozyme.

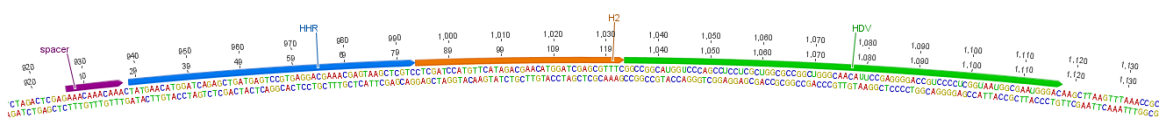


Figure 17: Structure and sequence of Plasmid H2 insert, including hammerhead ribozyme (HHR, blue), hairpin 2 (H2, orange), and hepatitis delta virus ribozyme (HDV, green).

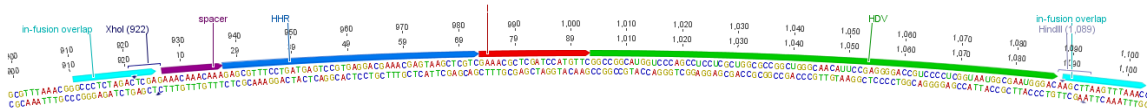


Figure 18. Structure and sequence of Plasmid I insert, including hammerhead ribozyme (HHR, blue), trigger RNA (I, red), and hepatitis delta virus ribozyme (HDV, green).

Once Plasmid H2 and Plasmid I were created, three clones were selected and sent for Sanger DNA sequencing. Next, we investigated whether the newly made plasmids correctly released H2 and I. All three clones were *in vitro* transcribed and analyzed for ribozyme cleavage. Clone 2 demonstrated the most efficient ribozyme cleavage for both plasmids (Figure 19).

While a band at 232 bp indicated that ribozyme cleavage was not 100% efficient in plasmid H2, the predicted fragments at 107 bp (the length from the T7 promoter to the HHR cleavage site) and 85 bp (the length from HDV cleavage site to the HindIII restriction site) were both observed. In addition, we saw a fragment 40 bp, demonstrating correct release of our sequence of interest.

Similar cleavage bands were observed for Plasmid I (Figure 19). A 209 bp fragment indicated that a significant portion of the plasmid was not cleaved. However, the presence of the desired 20 bp fragment demonstrated release of our sequence of interest in some cases.

Table 8: Expected size of all possible cleavage fragments of *in vitro* transcribed Plasmid H2.

Plasmid H2	
Size [bp]	Explanation
232	T7 to HindIII cut
147	T7 to H2 end (no HHR cleavage)
125	H2 + HDV to HindIII cut (no HDV cleavage)
107	T7 to HHR cleaved
85	HDV to HindIII cut
40	H2 (HHR/HDV cleaved)

Table 9: Expected size of all possible cleavage fragments of *in vitro* transcribed Plasmid I.

Plasmid I	
Size [bp]	Explanation
209	T7 to HindIII cut
124	T7 to I end (no HHR cleavage)
105	I + HDV to HindIII cut (no HDV cleavage)
104	T7 to HHR cleaved
85	HDV cleaved to HindIII cut
20	I (HHR/HDV cleaved)

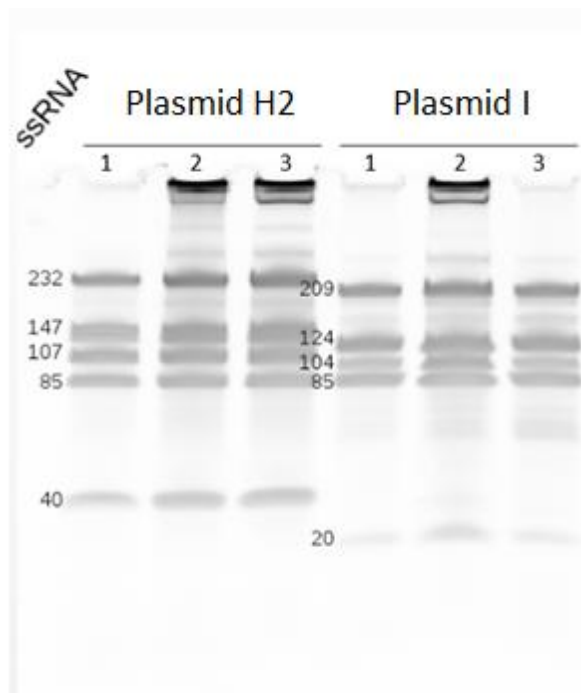


Figure 19: Analysis of the self-processing capacity ribozymes following *in vitro* transcription of Plasmid H2 and Plasmid I.

We demonstrated in the previous *in vitro* transcription tests that our target RNA sequences were released correctly from each plasmid. Next, we wanted to combine all three RNA HCR components that were cleaved from plasmids to evaluate their ability to polymerize. Following *in vitro* transcription, cleavage and separation by gel electrophoresis, we extracted our RNA sequences of interest (H1, H2, I), cleaned them and mixed them in HCR buffer. As demonstrated in Figure 20, long polymers of double-stranded RNA were formed.

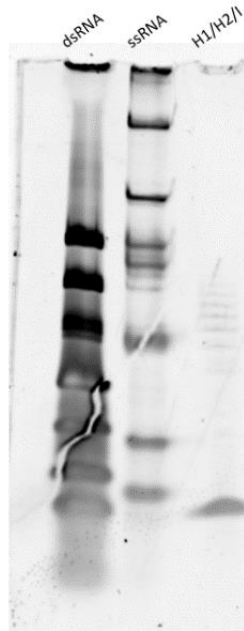


Figure 20: Hybridization chain reaction following combination of hairpin 1 (H1), hairpin 2 (H2) and trigger RNA (I) that were cleaved and released from plasmids H1, H2, and I.

Demonstrating HCR by RNA sequences cleaved from our designed plasmids was a major milestone in our study. To further optimize our plasmid constructs, we replaced the backbone of the plasmid with a Tet-One inducible vector. This inducible system allowed us to control expression of our plasmid using doxycycline. In addition, we combined both H1 and H2 in the same plasmid, leading to an even expression ratio of the two hairpins. Lastly, we included EGFP in our new plasmid, which allowed us to screen for correctly transfected cells (Figure 21).

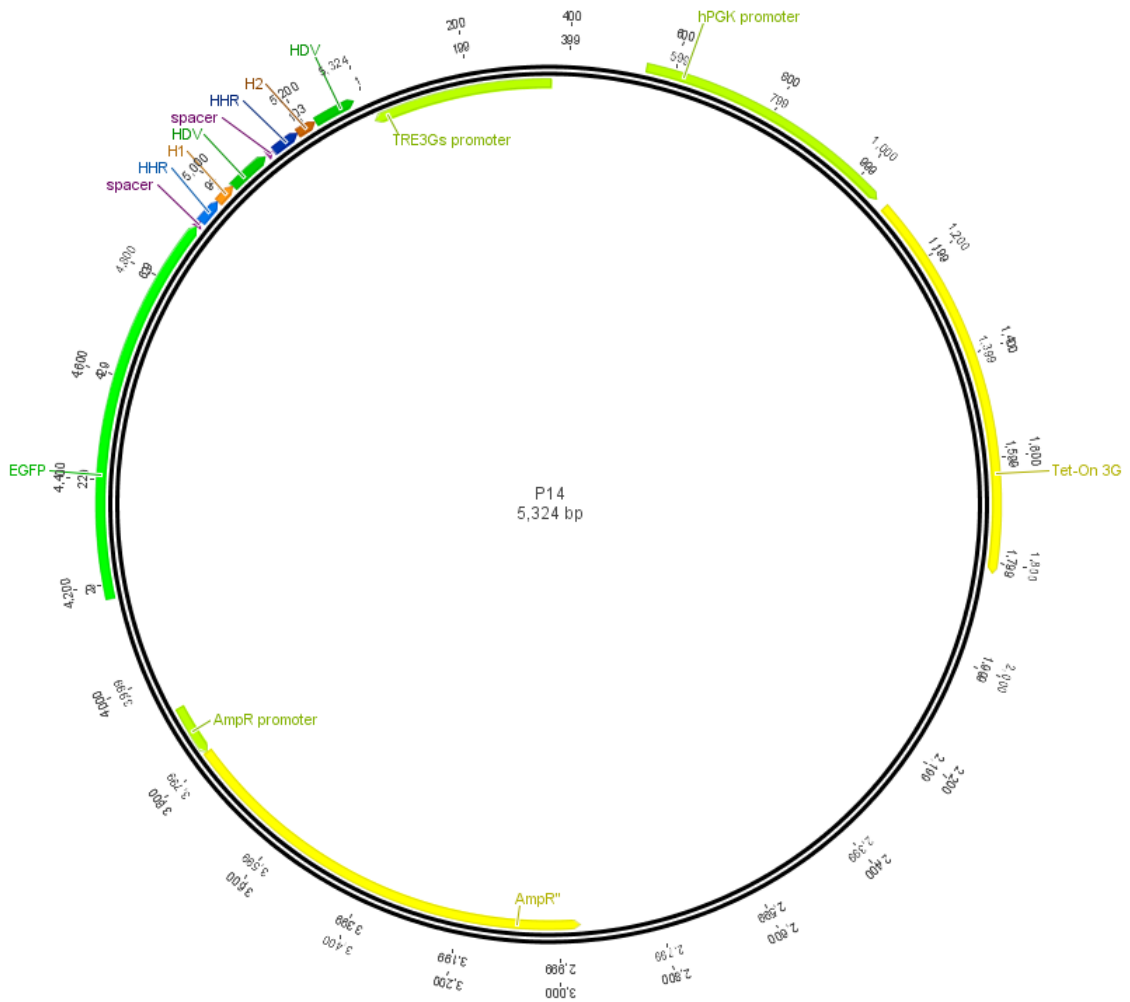


Figure 21A: Plasmid H1/H2 with EGFP (light green), hammerhead ribozyme 1 (HHR, light blue), hairpin 1 (H1, orange), hepatitis delta virus ribozyme (HDV, dark green), hammerhead ribozyme 2 (HHR, dark blue), hairpin 2 (H2, brown), and hepatitis delta virus ribozyme (HDV, dark green), and using a pTetOne vector as plasmid backbone.

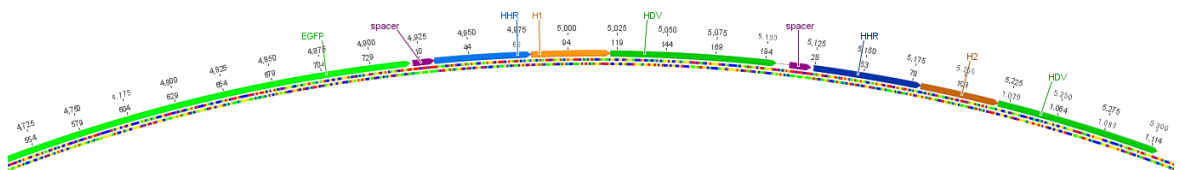


Figure 21B: Insert of Plasmid H1/H2: hammerhead ribozyme 1 (HHR, light blue), hairpin 1 (H1, orange), hepatitis delta virus ribozyme (HDV, dark green), hammerhead ribozyme 2 (HHR, dark blue), hairpin 2 (H2, brown), and hepatitis delta virus ribozyme (HDV, dark green).

Plasmid H1/H2 was created and sent for Sanger DNA sequencing. However, sequencing this plasmid turned out to be not successful. This was probably caused by the extended sequence homology shared by H1 and H2, which could lead to incorrect binding of the sequencing primers. Therefore, we decided to use selected fragment amplification to check whether the correct components were present in our plasmid. Of the five clones evaluated, only clone 3 did not yield our desired products.

On Figure 22A, the electrophoresis gel line marked “reaction 1” demonstrates the amplification of EGFP-specific product with band of 717 bp in size, indicating that it is present in Plasmid H1/H2. The band at 914 bp in reaction 2 indicates that the fragment including EGFP up to the first HDV is correctly represented. For reactions 3 and 4, we found PCR products at 1168 bp (the length from the beginning of EGFP to the second HDV) and at 440 bp (fragment from the end of EGFP to the second HDV). In the electrophoresis gel line marked “reaction 4”, the specificity of PCR reaction was low. This may be due to the fact that H1 and H2 share some sequence similarity, so the primers may attach to more than one site along the length of the insert. In conclusion, our desired products were present in plasmid H1/H2 and our PCR product sizes were able to confirm the results.

Table 10: Expected amplicon size of Plasmid H1/H2 PCR.

Using PCR to Check Plasmid H1/H2 Components	
Size [bp]	Explanation
717	EGFP
914	Beginning of EGFP to HDV ₁
1168	Beginning of EGFP to HDV ₂
440	End of EGFP to HDV ₂

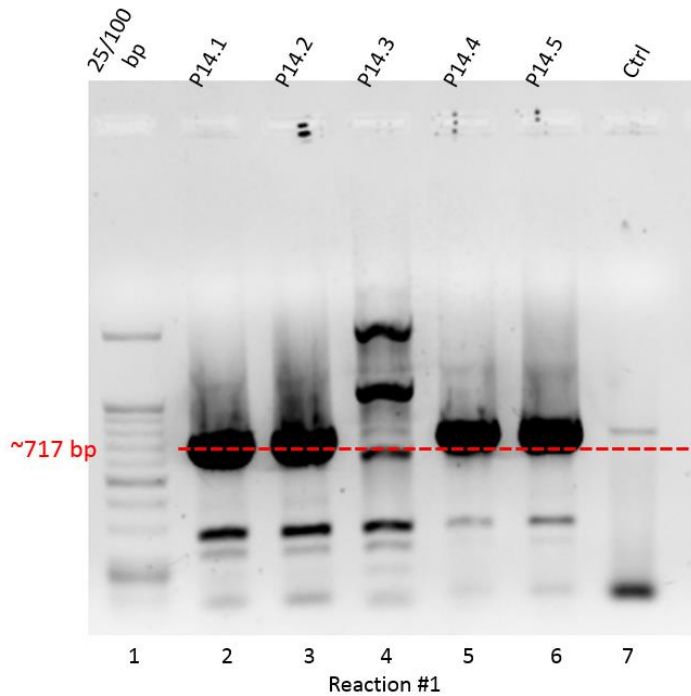


Figure 22A: PCR product of EGFP amplification from Plasmid H1/H2 clones 1, 2, 3, 4, 5 (see Table 10).

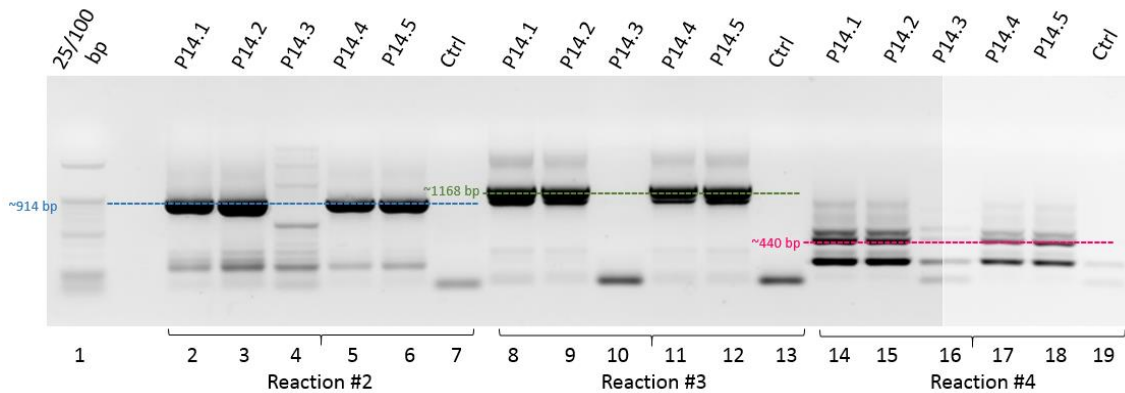


Figure 22B: PCR products of Plasmid H1/H2 clones 1, 2, 3, 4, 5 (see Table 10).

We now had an inducible plasmid that contains H1 and H2 components, and EGFP for easy screening of transfected cells. In a next step, we transfected PC3 cells with Plasmid H1/H2 and stimulated these cells with doxycycline that should, in theory,

induce EGFP expression and make the cells to fluoresce. Indeed, in the presence of doxycycline, cells transfected with plasmid H1/H2 became fluorescent (Figure 23).

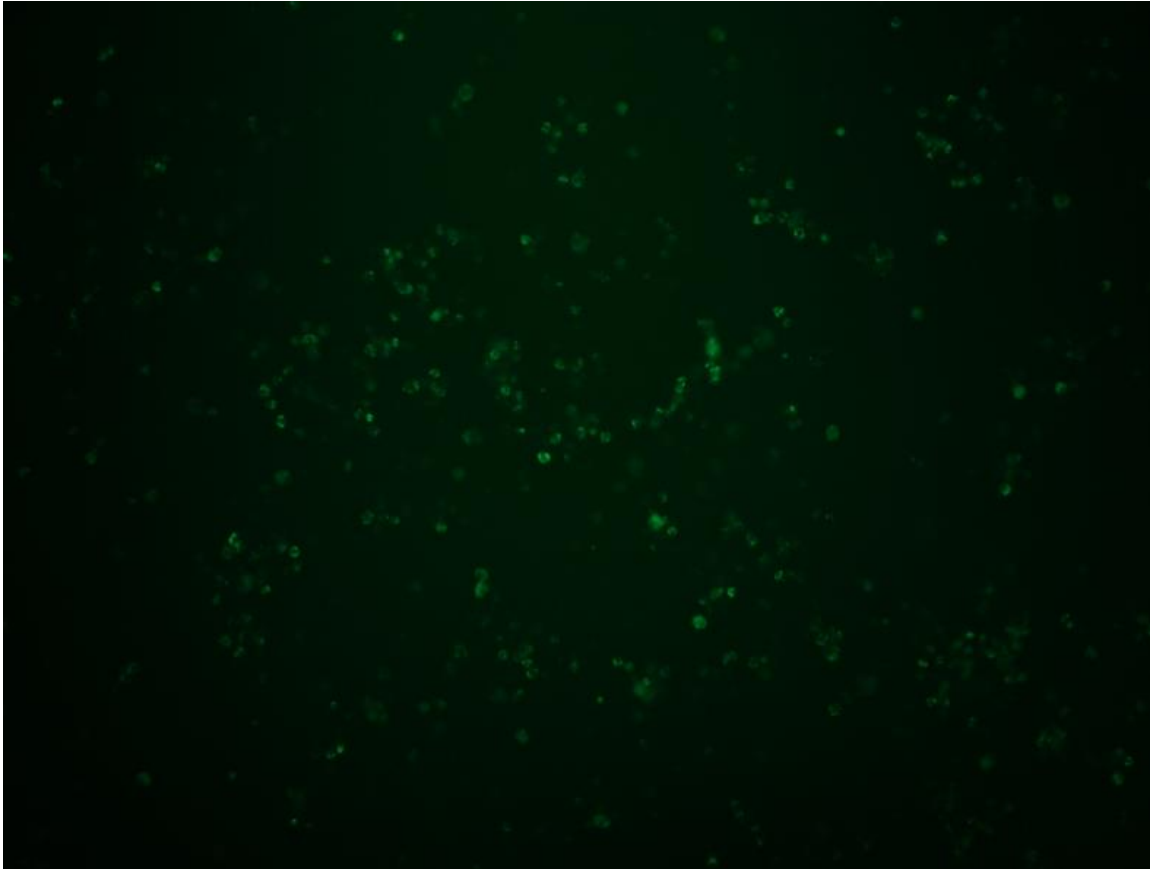


Figure 23: PC3 cells transfected with Plasmid H1/H2, and maintained in presence of doxycycline.

Development of a Gene Constructs that Enables Cell Fluorescence upon Receipt of a Trigger RNA:

In this Chapter, we describe the development of a second tool that allows recording of cell-cell communication using a trigger RNA. The original construct (plasmid A), contained a Cre-HHR-lox-STOP-lox-EGFP construct with a start codon

(ATG) immediately preceding EGFP (Figure 24A), causing strong false positive fluorescence in cells (Figure 27). Cells should only light-up when Cre protein is produced, and, therefore, the stop codon between loxP sites removed by Cre. After repositioning the ATG in front of the loxP-STOP-loxP site, a dramatic decrease in background fluorescence was observed (Figure 24B and Figure 28).

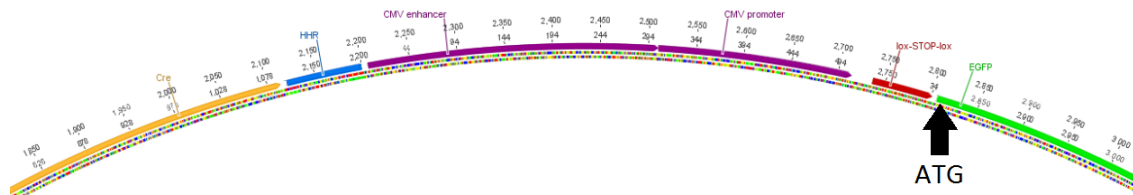


Figure 24A: Insert of plasmid A with ATG start codon in front of GFP.

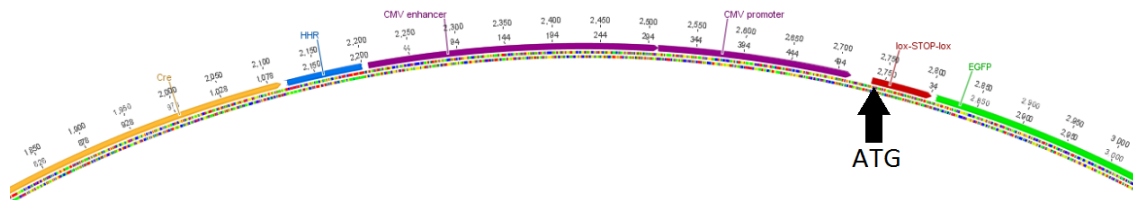


Figure 24B: Insert of plasmid B with ATG start codon in front of loxP-STOP-loxP site.

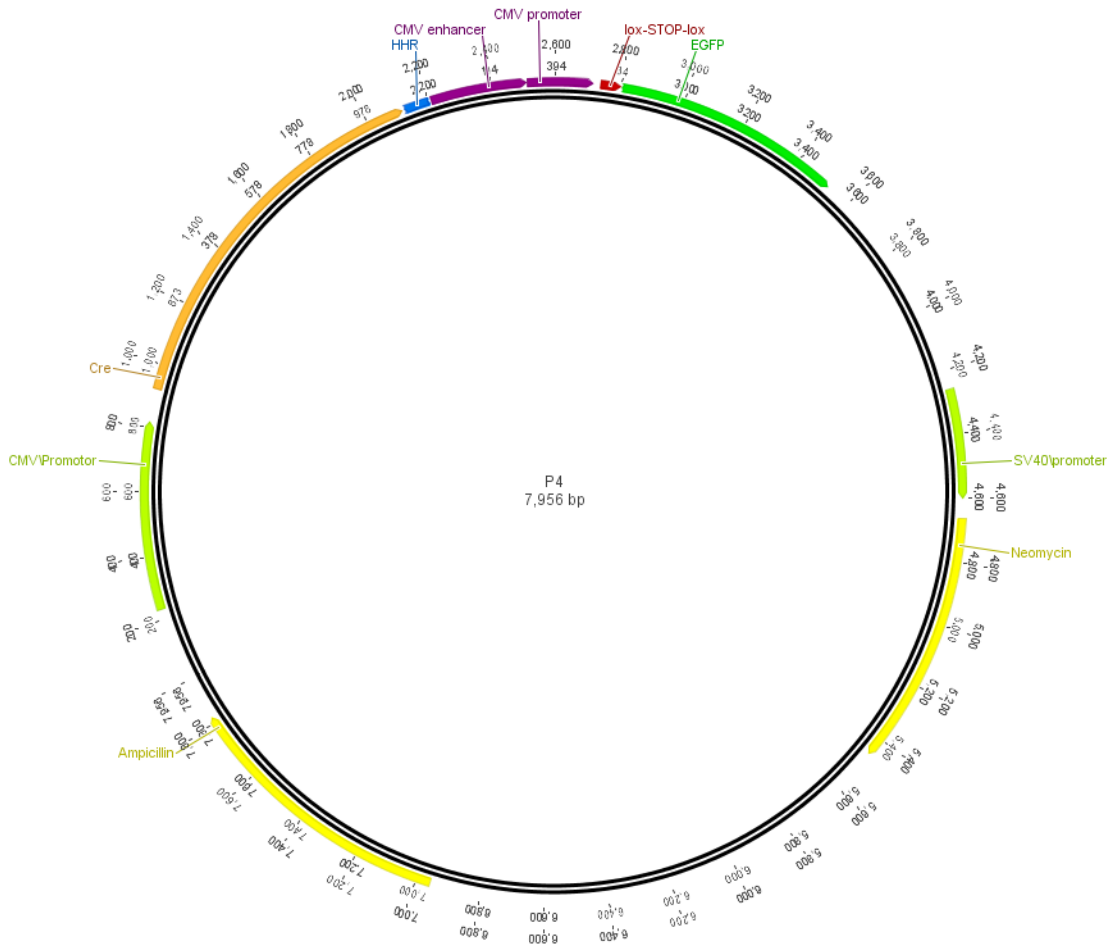


Figure 24C: Plasmid B with CMV promoter (light green), Cre recombinase (orange), hammerhead ribozyme (HHR, blue), CMV promoter 2 (purple), lox-STOP-lox site (red), and EGFP (dark green) in a pcDNA 3.1(-) vector.

To reposition the ATG start codon, we first amplified GFP without its start codon. We then used a 5' extension of the forward primer that amplified the loxP region to precede the loxP site with an ATG start codon (Figure 25A). After obtaining the PCR products of correct size, the fragments were cut out of the gel and cleaned for in-fusion cloning. Plasmid A was digested by

HindIII and HpaI to remove the insert that contained incorrectly positioned ATG start codon (Figure 25B).

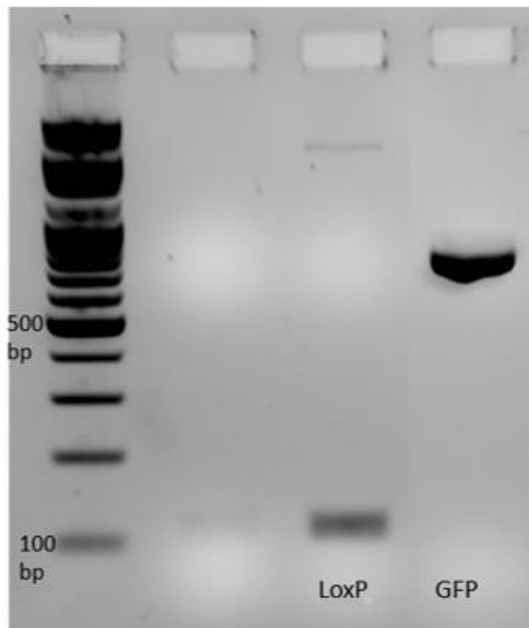


Figure 25A: Amplicon size of loxP with ATG and GFP sequence without ATG for in-fusion cloning.

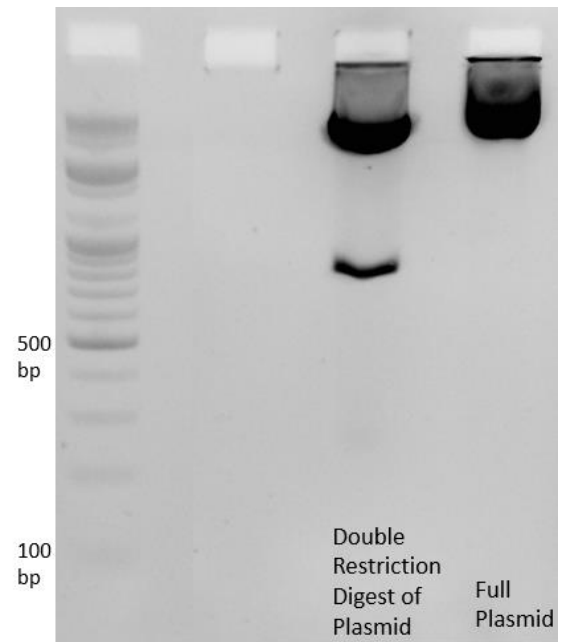


Figure 25B: Double restriction enzyme digestion of plasmid A for in-fusing cloning.

Following in-fusion cloning of the two inserts and the linearized plasmid, three clones were selected, and the plasmid DNA was extracted and sent for Sanger sequencing. According to sequencing results, Clone 1 contained the correct sequence with a new start codon (ATG) in front of the loxP site (Figure 26); Clone 2 contained

some non-related sequence (not shown); Clone 3 contained the desired insert with parts of the loxP site missing (Figure 26).

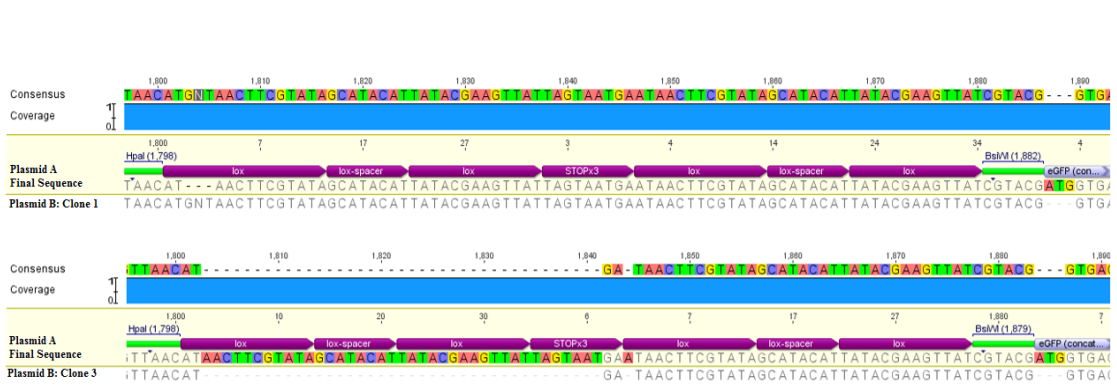


Figure 26: Sequence analysis of plasmid B, clones 1 and 3.

As expected, cells transfected with plasmid A, with the ATG start codon immediately preceding GFP, showed strong false positive fluorescence (Figure 27). On the other hand, in cells transfected with plasmid B, where the start codon was moved in front of the loxP site, a dramatic decrease in fluorescence was seen (Figure 28).

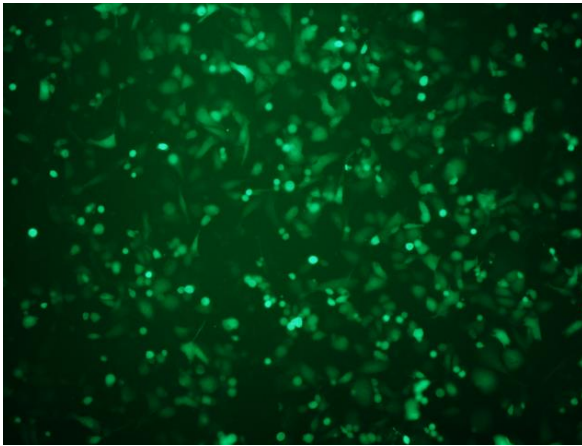


Figure 27: PC3 cells were transfected with Plasmid A (ATG start codon in front of GFP).

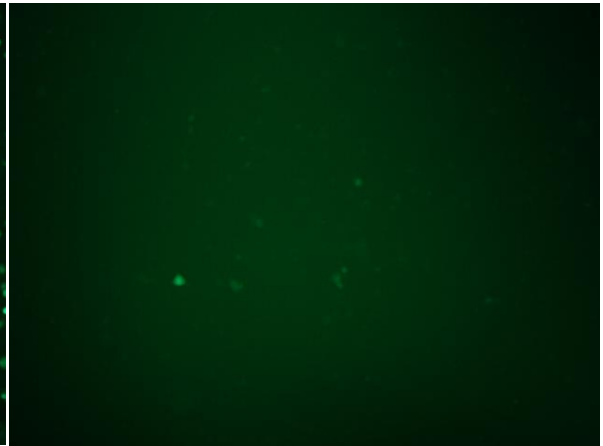


Figure 28: PC3 cells were transfected with Plasmid B (ATG start codon in front of lox-STOP-lox site).

However, some background fluorescence in cells transfected with plasmid B was evident (Figure 28). This may be due to the fact that the mechanism suppressing Cre expression³³ was working imperfectly, causing expression of Cre to leak. Therefore, Plasmid C was built, with a HHR at both the 5'- and 3'-end of Cre; that was done to ensure that Cre messenger RNA is cleaved, and that no Cre protein is produced (Figure 29).

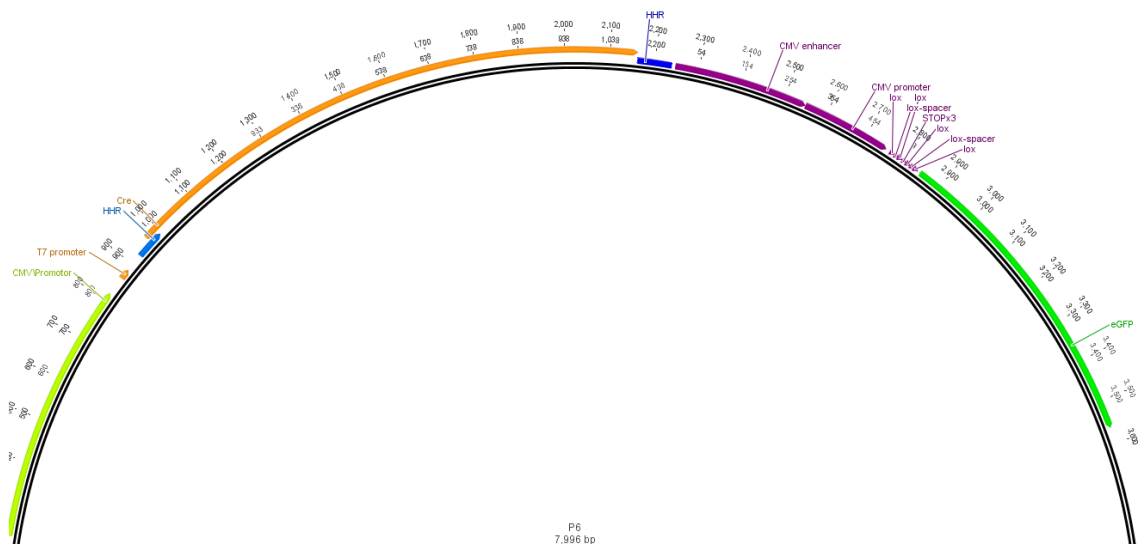


Figure 29: : Insert of Plasmid C: hammerhead ribozyme 1 (HHR, light blue), Cre (orange), hammerhead ribozyme 2 (HHR, dark blue), CMV promoter 2 (purple), lox-STOP-lox site (purple), and EGFP (dark green).

To verify the cleavage efficiency of both ribozymes, an *in vitro* transcription of plasmid C was performed. As shown in Table 11, a majority of expected product were 1 kb in size or larger. Figure 30 confirms that the majority of the RNA fragments had a high molecular weight and formed a thick band above 1,000 bp. This produces some difficulties or subsequent analysis in gel electrophoresis, as large RNA molecules run slowly, and are hard to size-separate. However, the observed band above 500 bp may represent the 3' HHR-to-HpaI cut site fragment. In addition, a 100-bp cleavage product was observed, this PCR product corresponds to the T7 promoter-to-5' HHR fragment.

Table 11: Expected size of all possible cleavage fragments following in vitro transcription of Plasmid C.

Plasmid C	
Size [bp]	Explanation
1878	T7 to HpaI cut site
1772	Cre to HpaI cut site (no 3'HHR cut)
1296	T7 to Cre end (no 5'HHR cut)
1192	Cre
580	3'HHR (post-Cre) to HpaI cut site
104	T7 to 5'HHR (pre-Cre)

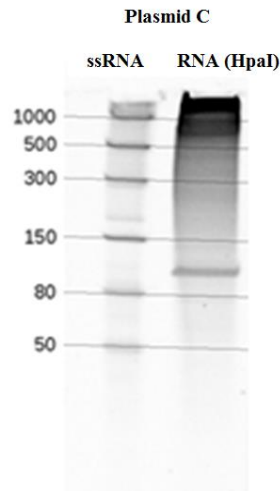


Figure 30: Cleavage fragments following in vitro transcription of Plasmid C.

To evaluate the cleavage efficiency of the HHR and HDV ribozymes in greater details, two two small fragments of plasmid C were amplified. Amplicon 1 had a length of 131 bp and included the T7 promoter until the end of 5'HHR (Figure 31A). Amplicon 2 started at the same site and stretched to the end of the 3'HHR, with a total length of 1363 bp (Figure 31B).

As shown in Figure 32, only lane 4 (clone 2) demonstrated correct 5'HHR cleavage, as evident by presence of bands at 106 bp and 25 bp. When analyzing cleavage efficiency in amplicon 2 (lanes 3, 5 and 7), we saw that again only clone 2 resulted in correct ribozyme cleavage. This was demonstrated by cleavage fragments of 106 bp (length from T7 promoter to 5' HHR) and 65 bp (length of 3'HHR) length.

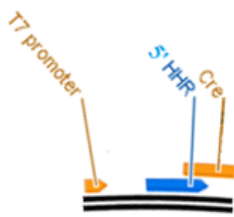


Figure 31A: Plasmid C, amplicon 1. Amplicon 1 contains the 5' hammerhead ribozyme (HHR) and starts at the T7 promoter and ends at the beginning of Cre. The total length of amplicon 1 is 131 bp.



Figure 31B: Plasmid C, amplicon 2. Amplicon 2 contains both hammerhead ribozymes (HHR) and starts at the T7 promoter and ends at the end of the 3' HHR. The total length of amplicon 2 is 1362 bp.

Table 12: Expected size of all possible cleavage fragments following in vitro transcription of amplicons 1 and 2 (see Figure 31)

Expected cleavage products (PLASMID C amplicon 1)	Size [bp]	Expected cleavage products (PLASMID C amplicon 2)	Size [bp]
T7 to end	131	T7 to end	1362
T7 to 5'HHR cut	106	T7 to 3'HHR cut (no 5'HHR cut)	1297
5'HHR cut to end	25	5'HHR cut to end (no 3'HHR cut)	1256
		5'HHR cut to 3'HHR cut	1191
		T7 to 5'HHR cut	106
		3'HHR cut to end	65

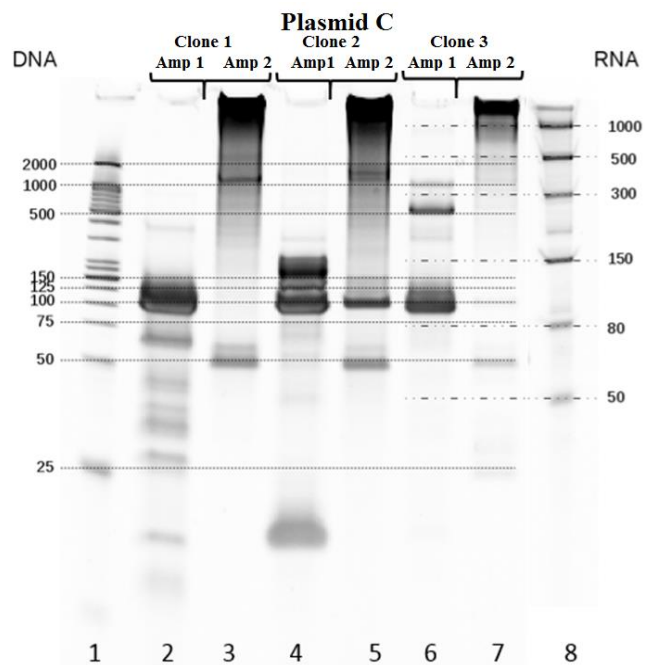


Figure 32: Cleavage fragments following in vitro transcription of amplicons 1 and 2 (see Table 12 and Figure 31)

Our next step was to investigate the optimal time point at which cleavage is the most visible. Oversaturation of gel bands would prevent evaluation of ribozyme cleavage

inhibition efficiency. As demonstrated in Figure 33A, the optimal time point to observe differences in ribozyme cleavage was within 5 to 10 minutes. Similar results were observed for cleavage of both amplicons, 1 and 2 (see Figure 33B). Therefore, to observe the biggest effect on ribozyme cleavage, a time point between 5 to 10 minutes was determined to be the optimal for stopping transcription in the presence of inhibitors.

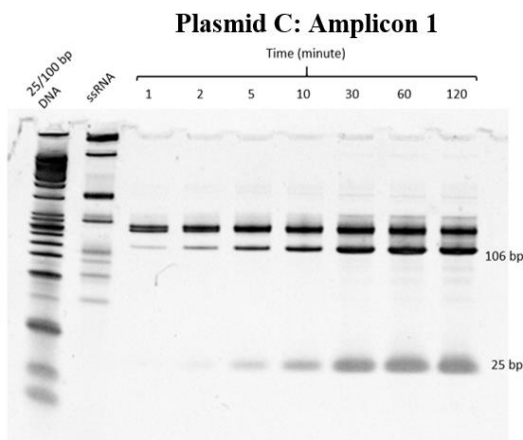


Figure 33A: In vitro transcription time course of amplicon 1 (see Figure 31).

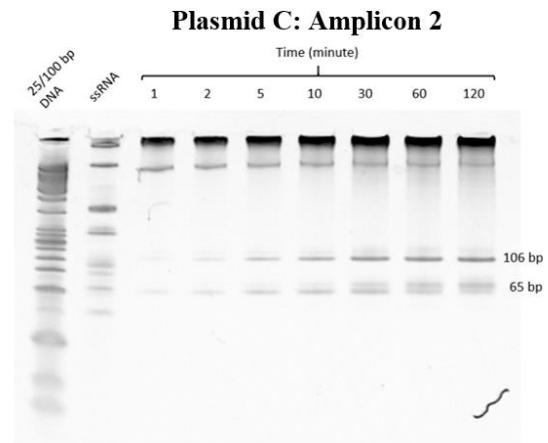


Figure 33B: In vitro transcription time course of amplicon 2 (see Figure 31).

To develop specific inhibitors against both ribozymes, *in silico* predicted complementary binding between ribozyme and inhibitor was evaluated experimentally. As shown in Figure 34, the 5' HHR contains stemloop I, II and III and has a cleavage site

between nucleotides guanine and cytosine. As compared to the 5' HHR, in 3' HHR, the stemloops are rotated, with the cleavage site being between cytosine and uracil. Inhibitors complementary to individual stemloops of the 5' HHR and 3' HHR were designed computationally, using the Geneious bioinformatics software (Figure 35). Expected locations of HHR inhibition are summarized in Table 12.

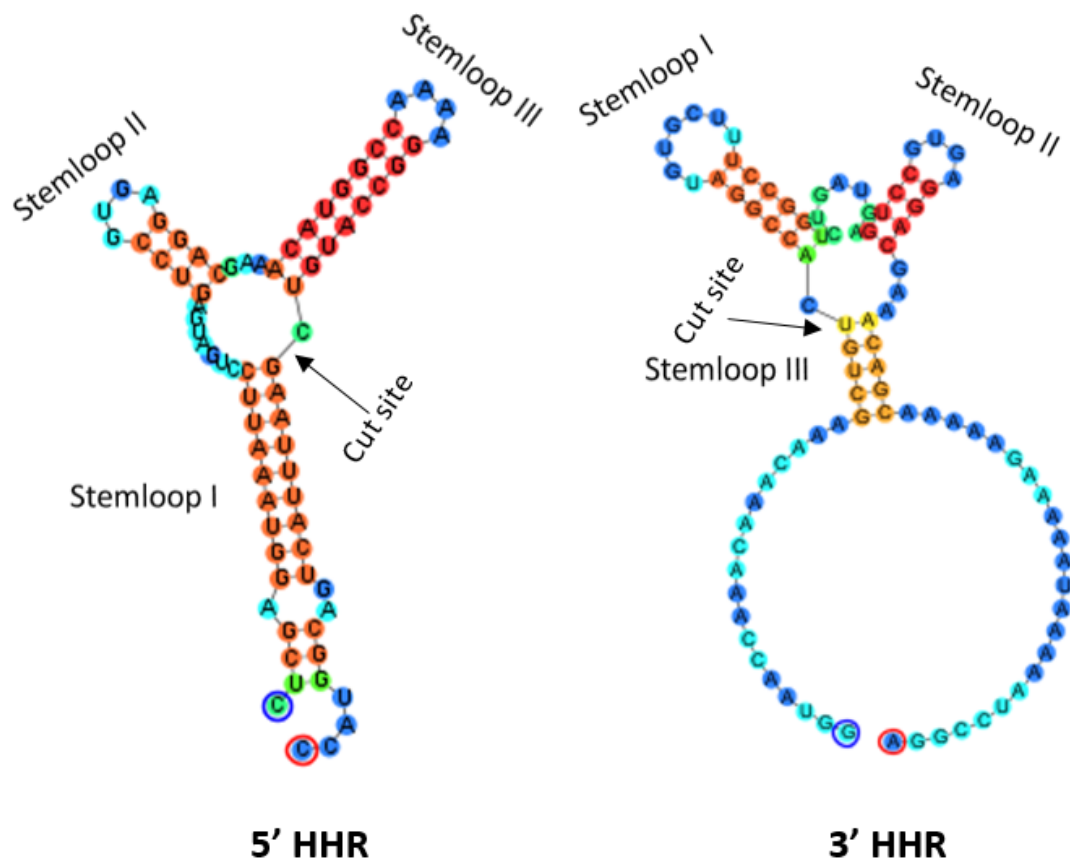


Figure 34: Structure of plasmid C 5' hammerhead ribozyme (HHR) and 3' HHR.

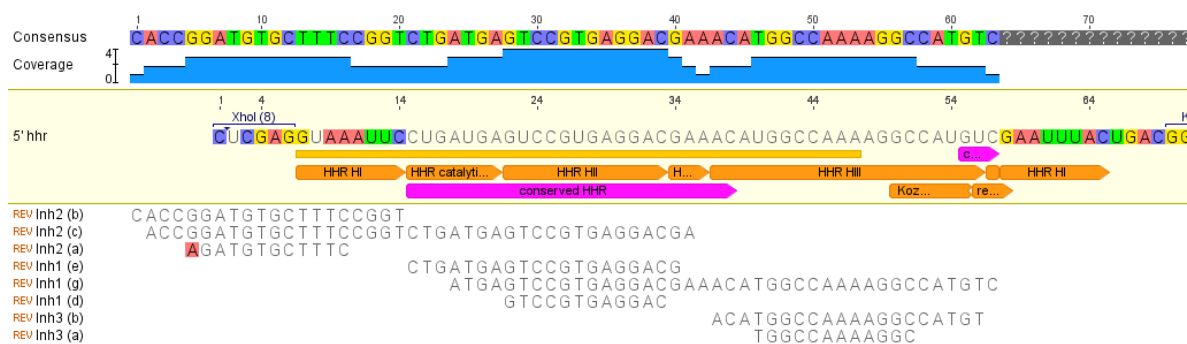


Figure 35A: Inhibitors complementary to stemloops of the 5' hammerhead ribozyme of plasmid C (see Figure 34).

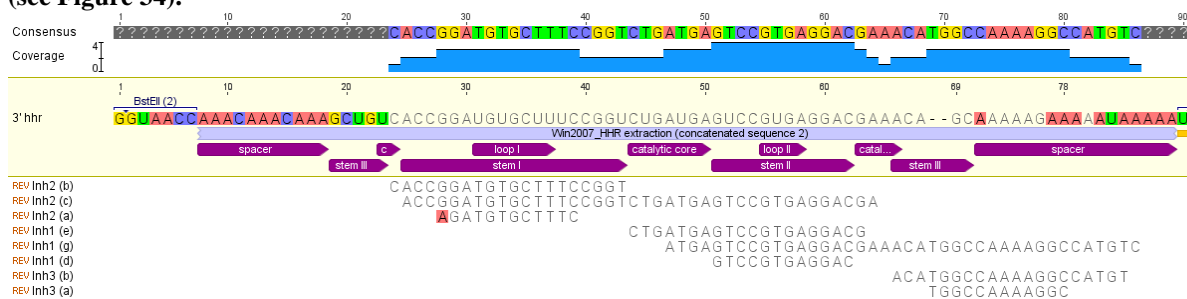


Figure 35B: Inhibitors complementary to stemloops of the 3' hammerhead ribozyme of plasmid C (see Figure 34).

Inhibitor	Size [bp]	Expected inhibition	Location
Inh1 (d)	12	Both HHRs	complementary to stemloop II which is equal in both HHRs
Inh1 (e)	20	Both HHRs	complementary to stemloop II which is equal in both HHRs
Inh1 (f)	20	No inhibition	Inhibitor is not complementary to HHRs
Inh1 (g)	40	Both HHRs	complementary to stemloop II which is perfect for 5' HHR and semi-perfect for 3' HHR
Inh2 (a)	12	3' HHR	complementary to stemloop I in 3' HHR
Inh2 (b)	20	3' HHR	complementary to stemloop I in 3' HHR
Inh2 (c)	40	Both HHRs More 3' HHR than 5' HHR	complementary to stemloop I and II which is perfect for 3' HHR and semi perfect for 5' HHR
Inh3 (a)	12	5' HHR	complement to stemloop III only in 5' HHR
Inh3 (b)	20	5' HHR	complement to stemloop III only in 5' HHR

Table 13: Inhibitor sets and predicted location of inhibition.

In order to confirm the ribozyme inhibition predicted *in silico*, an inhibition test was performed using selected inhibitors. The experiments were carried out at two time points, 5 minutes and 15 minutes, based on the previously determined optimal cleavage time (Figure 33). Gel electrophoresis of the products obtained in presence of all inhibitors showed strong bands at 106 bp (representing cleavage of the 5' HHR) and 65 bp (representing cleavage of the 3' HHR), indicating that ribozyme inhibition was not achieved.

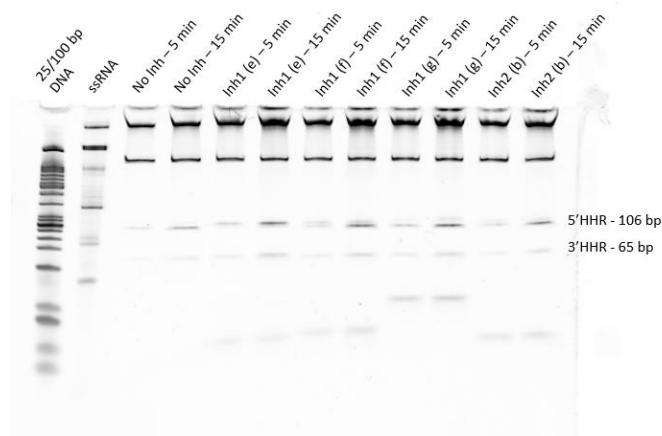


Figure 36: Ribozyme cleavage test of amplicon 2 (see Figure 31) following addition of selected inhibitors.

In order to better estimate the effects of the different inhibitors, and because RNA transcription and cleavage happen concurrently, each band was quantified separately, using ImageJ and obtained figures normalized it by the total RNA concentration in each sample. This provides more precise estimates of cleavage by the ratios of observed

cleavage products to the total RNA in each line. The fold difference in cleavage compared to cleavage without inhibitors at either 5 minutes or 15 minutes was then determined (Figure 37).

As shown in Figure 37A, the greatest inhibition of the 5' HHR was found at 15 minutes with inhibitor Inh1 (f). The same was true for the 3'HHR, with inhibitor Inh1 (f) being the most efficient. This was surprising, since inhibitor Inh1 (f) was predicted to have no effect and was originally included in our experiment as a negative control (Table 12). Further experiments will be necessary to thoroughly examine the cause of the false *in silico* prediction or whether any components in the reaction mix are prohibiting proper inhibitor-ribozyme interaction.

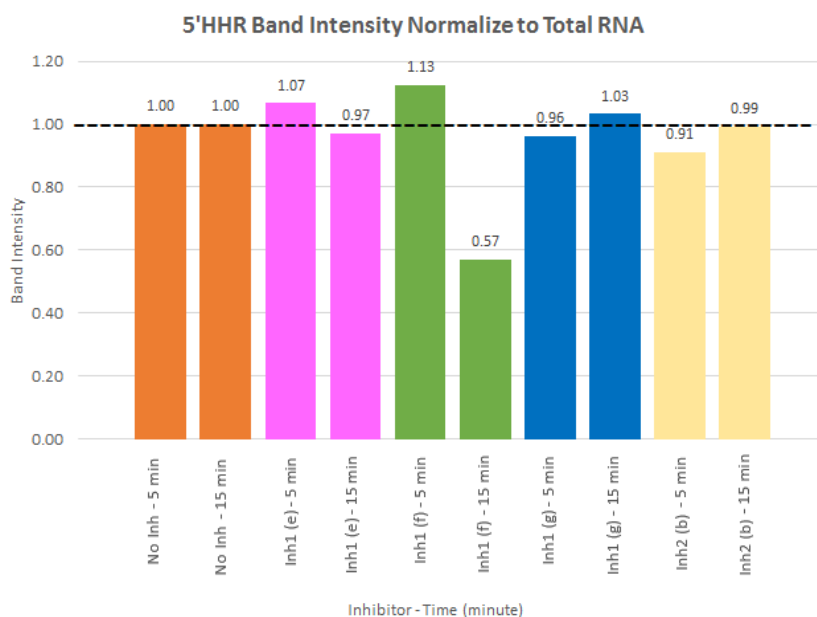


Figure 37A: 5' hammerhead ribozyme cleavage following addition of selected inhibitors (based on band intensity (see Figure 36)).

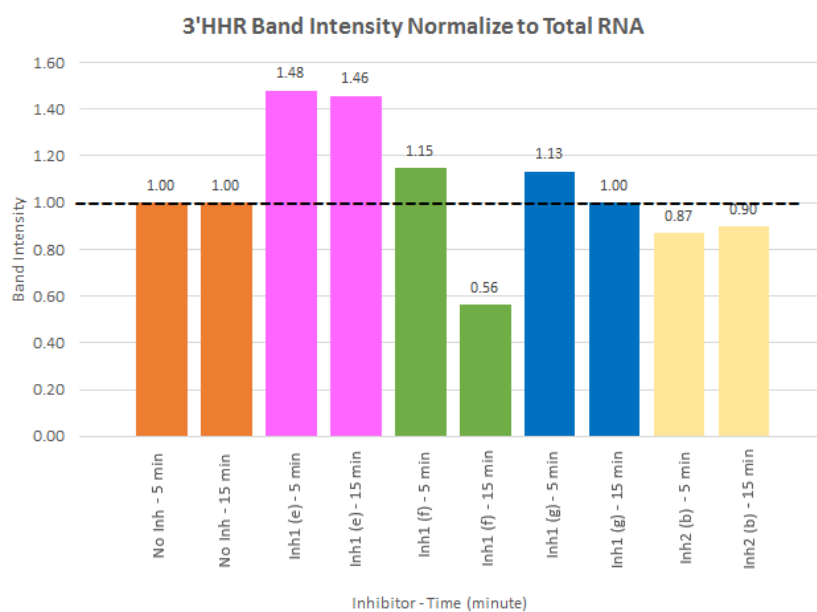


Figure 37B: 3' hammerhead ribozyme cleavage following addition of selected inhibitors (based on band intensity (see Figure 36)).

IV CONCLUSION

Our studies demonstrate the ability of the hybridization chain reaction mechanism to mediate cell death in cultured human cancer cells. To illustrate this, we first developed and optimized sets of DNA oligonucleotides that emulate RNA hybridization behavior. Candidates producing successful HCR were identified and results replicated using analog RNA oligonucleotides. Notably, test tube experiments suggested that the presence of trigger RNA is critical for the chain reaction between hairpin 1 and hairpin 2 to occur. However, transfection of cancer cells with hairpins 1 and 2 together with or without trigger RNA caused cell death. Further experiments revealed that the native RNA present in these cells is capable of acting as trigger RNA. In fact, total RNA extracted from cells was able to act as trigger RNA for HCR in a test tube experiments, albeit much less efficiently than specially designed trigger RNA.

To address the problem of maintaining even ratios of hairpins 1 and 2 in receiver cells and to prohibit silencing of the transfected constructs, a plasmid was generated that contained hairpin 1 and 2 sequences in a Tet-One inducible vector. In addition, the plasmid contained EGFP was developed to allow for quick screening of transfected cells by fluorescence microscopy. *In vitro* transcription assays of the plasmid demonstrated the correct cleavage of hairpins 1 and 2 by flanking hammerhead and hepatitis delta virus

ribozymes. Prostate cancer cells transfected with this plasmid demonstrated green fluorescence in the presence of doxycycline, indicating efficiency of transfection.

Further, we created a Cre recombinase gene construct, flanked by two hammerhead ribozymes, which can be specifically inhibited using a short trigger oligonucleotide. This construct also contained a loxP-STOP-loxP site followed by a GFP sequence, allowing for the Cre-dependent expression of GFP. In studies with a start codon (ATG) placed directly in front of GFP, we observed strong false positive fluorescence in cells. After repositioning the ATG in front of the loxP-STOP-loxP site, a dramatic decrease in fluorescence was observed, demonstrating that the loxP-STOP sequence functions correctly. *In vitro* transcription of this construct showed high efficiency of cleavage for both ribozymes, resulting in the excision and downregulation of Cre.

Following the demonstration of ribozyme functioning within the gene construct, inhibitors were synthesized to prevent ribozyme cleavage. However, we found a discrepancy between *in silico* prediction of inhibitor-ribozyme binding and actual ribozyme inhibition in *in vitro* experiments. This suggests that the predicted *in silico* inhibitor-ribozyme binding events are not sufficient to explain inhibitor-ribozyme interactions *in vivo*. To optimize inhibitors and achieve complete inhibition of ribozyme cleavage, additional experimentation is required

However, already at that stage of the optimization process, both technologies clearly show promise to become critical tools for visualizing RNA-based cell-cell

communication. Further development of both techniques will provide a means to not only observe and quantify RNA-based cell-cell communication *in vivo*, but also determine how dependent tumor development is on stromal cells that surrounds the cancer cells and embed them in their communicative milieu.

REFERENCES

1. Norman, J.M.V., Breakfield N.W. & Benfey P.N. Intercellular Communication during Plant Development. *Plant Cell*. **23**, 855–64 (2011).
2. Marx V. Cell communication: stop the microbial chatter. *Nature*. **511**, 493–7 (2014).
3. Giaouris, E., Heir, E., Desvaux, M., Hébraud, M., Møretrø, T., Langsrud, S., et al. Intra- and inter-species interactions within biofilms of important foodborne bacterial pathogens. *Front Microbiol*. **6**, 841 (2015).
4. Hentzer, M., Eberl, L., Nielsen, J. & Givskov, M. Quorum sensing : a novel target for the treatment of biofilm infections. *BioDrugs Clin Immunother Biopharm Gene Ther*. **17**, 241–50 (2003).
5. Potera, C. Biofilms invade microbiology. *Science*. **273**, 1795–7 (1996).
6. Agur, Z., Kogan, Y., Levi, L., Harrison, H., Lamb, R., Kirnasovsky, O.U., et al. Disruption of a Quorum Sensing mechanism triggers tumorigenesis: a simple discrete model corroborated by experiments in mammary cancer stem cells. *Biol Direct*. **5**, 20 (2010).
7. DeWys, W.D. Studies correlating the growth rate of a tumor and its metastases and providing evidence for tumor-related systemic growth-retarding factors. *Cancer Res*. **32**, 374–9 (1972).
8. Fisher, B., Gunduz, N., Coyle, J., Rudock, C. & Saffer, E. Presence of a growth-stimulating factor in serum following primary tumor removal in mice. *Cancer Res*. **49**, 1996–2001 (1989).
9. Joyce, J.A. & Pollard, J.W. Microenvironmental regulation of metastasis. *Nat Rev Cancer*. **9**, 239–52 (2009).
10. Sceneay, J., Chow, M.T., Chen, A., Halse, H.M., Wong, C.S.F., Andrews, D.M., et al. Primary tumor hypoxia recruits CD11b+/Ly6Cmed/Ly6G+ immune suppressor cells and compromises NK cell cytotoxicity in the premetastatic niche. *Cancer Res*. **72**, 3906–11 (2012).
11. Cleary, A.S., Leonard, T.L., Gestl, S.A. & Gunther, E.J. Tumour cell heterogeneity maintained by cooperating subclones in Wnt-driven mammary cancers. *Nature*. **508**, 113–7 (2014).
12. Chapman, A., Fernandez Del Ama, L., Ferguson, J., Kamarashev, J., Wellbrock, C. & Hurlstone, A. Heterogeneous tumor subpopulations cooperate to drive invasion. *Cell Rep*. **8**, 688–95 (2014).
13. Quail, D.F. & Joyce, J.A. Microenvironmental regulation of tumor progression and metastasis. *Nat Med*. **19**, 1423–37 (2013).

14. Qian, Z., Shen, Q., Yang, X., Qiu, Y. & Zhang, W. The Role of Extracellular Vesicles: An Epigenetic View of the Cancer Microenvironment. *BioMed Res Int.* **20**, 649161 (2015).
15. He, L. & Hannon, G.J. MicroRNAs: small RNAs with a big role in gene regulation. *Nat Rev Genet.* **5**, 522–31(2004).
16. Patton, J.G., Franklin, J.L., Weaver, A.M., Vickers, K., Zhang, B., Coffey, R.J., et al. Biogenesis, delivery, and function of extracellular RNA. *J Extracell Vesicles.* **4**, 27494 (2015).
17. Katakowski, M., Buller, B., Wang, X., Rogers, T. & Chopp, M. Functional microRNA is transferred between glioma cells. *Cancer Res.* **70**, 8259–63 (2010).
18. Valiunas, V., Polosina, Y.Y., Miller, H., Potapova, I.A., Valiuniene, L., Doronin, S., et al. Connexin-specific cell-to-cell transfer of short interfering RNA by gap junctions. *J Physiol.* **568**, 459–68 (2005).
19. Hammann, C., Luptak, A., Perreault, J., & de la Pena, M. The ubiquitous hammerhead ribozyme. *RNA.* **18**, 871-885 (2012).
20. Pley, H.W., Flaherty, K.M., & McKay, D.B. Three-dimensional structure of a hammerhead ribozyme. *Nature.* **372**, 68-74 (1994).
21. Been, M.D. & Wickham, G.S. Self-cleaving ribozymes of hepatitis delta virus RNA. *Eur. J. Biochem.* **247**, 741-753 (1997).
22. Ferré-D'Amaré, A.R. & Doudna, H.A. Use of *cis*- and *trans*-ribozymes to remove 5' and 3' heterogeneities from milligrams of *in vitro* transcribed RNA. *Nucleic Acid Research.* **24**, 977-978 (1996).
23. Gao, Y. and Zhao, Y. Self-processing of ribozyme-flanked RNAs into guide RNAs *in vitro* and *in vivo* for CRISPR-mediated genome editing. *JIPB.* **56**, 343-349 (2014).
24. Walker, S.C., Avis, J.M., & Conn, G.L. General plasmids for producing RNA *in vitro* transcripts with homogenous ends. *Nucleic Acids Research.* **31**, 1-6 (2003).
25. Isaacs, F.J., Dwyer, D.J., Ding, C., Pervouchine, D.D., Cantor, C.R., Collins, J.J. Engineered riboregulators enable post-transcriptional control of gene expression. *Nat Biotechnol.* **22**, 841–7 (2004).
26. Dirks, R.M. & Pierce, N.A.. Triggered Amplification by Hybridization Chain Reaction. *Proc Natl Acad Sci USA.* **101**, 15275-15278 (2004).
27. García, M.A., Meurs, E.F., Esteban, M. The dsRNA protein kinase PKR: virus and cell control. *Biochimie.* **89**, 799–811 (2007).
28. Kumar, M. & Carmichael, G.G. Antisense RNA: function and fate of duplex RNA in cells of higher eukaryotes. *Microbiol Mol Biol Rev MMBR.* **62**, 1415–34 (1998).
29. Wang, Q. & Carmichael, G.G. Effects of Length and Location on the Cellular Response to Double-Stranded RNA. *Microbiol Mol Biol Rev.* **68**, 432–52 (2004).
30. Jaisser, F. Inducible gene expression and gene modification in transgenic mice. *J Am Soc Nephrol.* **11**, S95–S100 (2000).
31. Schindelin, J., Arganda-Carreras, I., Frise E, Kaynig, V., Longair, M., Pietzsch, T., et al. Fiji: an open-source platform for biological-image analysis. *Nat Methods.* **9**, 676–82 (2012).

32. Venkataraman, S., Dirks, R.M., Ueda, C.T., & Pierce NA. Selective cell death mediated by small conditional RNAs. *Proc Natl Acad Sci USA*. 107, 16777-82 (2010).
33. Win, M.N. & Smolke, C.D. A modular and extensible RNA-based gene-regulatory platform for engineering cellular function. *PNAS*. 104, 14283-88 (2007).

CURRICULUM VITAE

Cindy T. Duong graduated from George Mason University in spring 2011 with a Bachelor of Science in biology and a minor in Business.